UNIVERSIDADE DE LISBOA
FACULDADE DE CIÊNCIAS
DEPARTAMENTO DE BIOLOGIA ANIMAL

Establishing 3D models to dissect the role of basement membrane-cell communication in cancer

João Pedro Nunes Ferreira

Mestrado em Biologia Evolutiva e do Desenvolvimento

Dissertação orientada por:
Prof. Dra. Ana Rita Cabral Martins Carlos
Prof. Dra. Rita Zilhão

2024

Acknowledgements

I would like to begin by saying that I am not good with this kind of thing. It has never been my forte to put any sort of feeling or emotion to paper. It would be easier for me to not write this but that would not be fair to the people who have helped me on this rollercoaster of a journey. So, here goes.

First, I would like to thank my advisors, Prof. Dr. Ana Rita Carlos and Prof. Dr. Rita Zilhão, for letting me do this project in their lab, under their guidance. Your support was invaluable in successfully getting me to the end, not just in terms of insight and knowledge, but also in your encouragement when things did not go as planned.

Second, I would like to thank the other members of the EMDD and MMD labs. You were fantastic colleagues, always willing to help and give advice when needed. As someone likes to say, a true 'closed pinecone' of a lab. Here I must give a special thanks to Vanessa, for working closely with me on this project, teaching me the fundamentals of working in the lab and for enduring my most pessimistic moments. Another special thanks goes to Diogo for his expertise and help in molecular cloning and transfection, as well as his ability to lift everyone's spirits.

Another big thank you goes to Marta Palma and Dr. Joaquim Tapisso, from whom I have learned a lot while working as a monitor. Thanks to you it was a great and invaluable experience, which I will never forget.

I would also like to thank all the friends that have been with me on this journey. Being able to talk to you during lunch, in the cell culture room or even just by text means a lot to me, just like your friendship, even if I may not always show it. I am deeply honoured to be able to call you all my friends and even if nothing else comes from this adventure at least I got to meet you.

Last but not least, I want to thank my family. My parents, who have always believed in me and have been supporting me and my dreams from the beginning. My brother, who despite at times being a little annoying, still encourages and eggs me on in his own way. My uncle and cousins, who so graciously welcomed me into their home so I could study and pursue my passions. I could not have asked for a better, more loving family, so thank you for everything, from the bottom of my heart.

Abstract

Like all cancers, melanoma is a multifactorial disease characterised by several cancer hallmarks. Previously thought to be a support structure, the extracellular matrix (ECM) is now known to govern many of the processes related to these hallmarks, such as cell proliferation, apoptosis and invasion. Therefore, understanding the role of this structure in tumour progression is paramount to deepening our knowledge of this disease. *In vitro* models are a fundamental part of this research; however, classical two-dimensional monolayer cell cultures are known to not accurately represent the ECM. Three-dimensional (3D) models are better at this, since they allow the formation of the complex cell-cell and cell-matrix interactions that are vital to evaluate the impact of the ECM. This project aimed to establish spheroids, a type of 3D model, to study the effect of ECM mutations in tumour progression, focusing on the effects of *LAMA2* abnormalities, a key ECM component. In this project we showed that the A375 human melanoma cell line was able to form spheroids, and this characteristic was not altered in the context of *LAMA2* knockout (KO) or *LAMA2* overexpression (OE). These spheroids were characterized in terms of cell proliferation, cell death, growth and the expression of some genes of interest (GOIs). Results indicated that most cells in each spheroid were viable during the time of the analysis, suggesting the feasibility of the models used. No differences were found in proliferation, cell death, growth or the expression of the analysed genes due to *LAMA2* absence or overexpression. ECM and ECM related components were also analysed. Fibronectin levels appeared to be correlated with laminin-α2 presence, since less laminin-α2 led to a decrease in fibronectin. Overall, this project lays the foundation for the use of spheroid models to the study the role of the ECM and *LAMA2* in tumour progression.

Keywords: Melanoma, Spheroids, *LAMA2*, Overexpression, Extracellular matrix

Resumo Alargado

O cancro tem vindo a tornar-se um dos maiores desafios sociais, económicos e de saúde pública no século XXI. Esta patologia é já a segunda causa de morte prematura causada por doenças não-transmissíveis em vários países e prevê-se que esta situação se venha a agravar. Um dos tipos de cancro que mais rapidamente tem aumentado é o melanoma, um cancro da pele, que em 2022 foi o 17º cancro mais diagnosticado a nível global. Esta doença advém de alterações genéticas e epigenéticas em melanócitos, células encontradas em vários tecidos onde desempenham diversas funções. Na camada basal da epiderme a principal função destes melanócitos é a produção de melanina, pigmento que absorve e dispersa radiação ultravioleta, danificadora do DNA, o que é extremamente importante na pele, cujas células são regularmente expostas a esta radiação.

As alterações que levam à transformação de melanócitos em melanoma são resultado de vários fatores extrínsecos e intrínsecos. Assim o melanoma é, como todos os cancros, uma doença complexa e multifatorial, que pode ser caracterizada por uma série de caracteres denominados *cancer hallmarks*. Estes definem as características biológicas fundamentais adquiridas durante a progressão tumoral que caracterizam o aparecimento do cancro. Exemplos incluem proliferação contínua, resistência à apoptose, imortalidade replicativa, angiogénese e ativação de invasão e metástase.

A matriz extracelular (ECM) é uma rede acelular complexa composta por várias moléculas. As mais abundantes são colagénios, elastina, glicoproteínas (como fibronectina e lamininas) e proteoglicanos. Tradicionalmente a ECM era vista como uma simples estrutura de suporte, mas hoje sabe-se que as suas funções são muito mais complexas. Para além do suporte mecânico a ECM é também responsável por regular processos fundamentais para a manutenção da homeostase de células e tecidos, incluindo proliferação, diferenciação e migração celular. Dado este papel fundamental não é surpreendente que alterações na estrutura e composição da ECM tenham uma grande importância na modulação dos acima mencionados *cancer hallmarks*. Por exemplo, sabe-se que deposição excessiva de certos componentes da matriz, comum em vários tipos de cancro, leva ao aumento da sua rigidez, que por sua vez promove aumento da proliferação celular, resistência à apoptose e angiogénese. Por outro lado, uma remodelação excessiva da ECM pode levar ao enfraquecimento da membrana basal e assim facilitar a invasão de tecidos. Outras alterações da matriz podem ainda facilitar a tumorigénese através do aumento da instabilidade genómica, como certas mutações em colagénios.

Tendo em conta a função crítica da ECM na progressão tumoral torna-se prioritário estudar a forma como alterações nesta estrutura afetam esta progressão para aprofundar o conhecimento desta doença. Para tal modelos *in vitro* são fundamentais. Este tipo de modelo biológico tem sido usado em investigação há décadas, tendo sido usados para compreender um grande número de processos e mecanismos biológicos, tanto em homeostase como em doença. Culturas de células em monocamada bidimensionais (2D) são um dos modelos mais usados, devido à sua simplicidade, consistência e conveniência. Várias descobertas relativas aos *cancer hallmarks* foram feitas nestes modelos e têm sido regularmente usados no processo de teste de novas drogas e agentes quimioterapêuticos. Não obstante o seu uso extensivo, existem vários aspetos em que estes modelos 2D não representam fielmente a condição *in vivo*. É frequente células cultivadas em monocamada terem funções biológicas alteradas, com propriedades como proliferação, apoptose, metabolismo e regulação transcricional de algum modo diferentes em relação ao que é observado *in vivo*. Devido a estas diferenças os resultados obtidos com estes modelos podem ter um poder preditivo pobre. Culturas 2D são especialmente ineficientes no que se refere a simular a ECM, uma vez que o seu modo de crescimento limita as interações célula-célula e previne o estabelecimento de uma ECM. Deste modo modelos 2D não são apropriados para o estudo de questões que envolvam a ECM. Para tal modelos tridimensionais (3D) apresentam-se como uma melhor alternativa. Este tipo de modelo permite o crescimento de células num ambiente 3D e,

consequentemente, o estabelecimento de mais e mais complexas interações célula-célula e célula-matriz. Um tipo de modelo 3D comumente usado são esferoides. Estes consistem em agregados de células flutuantes, que se sabe produzirem a sua própria ECM. Além disso, por serem 3D, existe o estabelecimento de um gradiente de nutrientes, pH e oxigénio do exterior para o interior do esferoide, o que é especialmente apropriado para o mimetismo de tumores sólidos. Estes modelos são relativamente baratos e fáceis de usar e por isso têm sido usados para explorar diversos aspetos relacionados com o cancro, como por exemplo invasão e resposta a tratamentos. Dito isto torna-se claro que para explorar o papel da ECM na progressão tumoral o uso de modelos 3D, como esferoides, será uma escolha vantajosa.

Neste sentido o objetivo principal deste projeto foi o estabelecimento de esferoides com células de melanoma para investigar o papel da ECM e suas alterações, especificamente em *LAMA2*, que codifica para a cadeia α2 das lamininas. Para tal foram inicialmente testados dois métodos de geração de esferoides, usando células A375 (uma linha celular de melanoma humano) *wild-type* (WT): *hanging drops*, em que a formação de esferoides é promovida pela gravidade, e *agarose-coated wells*, em que poços de uma placa de 96-poços são cobertos em agarose que impede a aderência de células ao fundo e por isso promove a formação de esferoides. Foi possível gerar esferoides através de ambos os métodos, no entanto os esferoides gerados por *hanging drops* aparentaram ser menos coesos e mais frágeis. Esse facto, adicionado à necessidade de maior manipulação, levou a que o método *agarose-coated wells* fosse escolhido para gerar esferoides em experiências subsequentes. Após determinar o melhor método para a sua obtenção, esferoides gerados usando células A375 WT e *LAMA2 knockout* (KO) foram caracterizados em termos de crescimento, proliferação e morte celular. Não foram observadas diferenças significativas em qualquer um destes parâmetros entre linhas celulares. Tanto o crescimento como a proliferação se mantiveram constantes durante o período experimental e a morte celular observada foi notavelmente baixa, não ultrapassando os 2% em qualquer uma das linhas. Estes esferoides foram ainda usados para analisar o impacto da ausência de *LAMA2* noutras proteínas da ECM e na comunicação célula-ECM. Através de imunofluorescência foi determinado que esferoides *LAMA2*-KO apresentam menos laminina-α2 que esferoides WT, como esperado, e que os níveis de fibronectina parecem seguir o mesmo padrão. Não foram observadas diferenças nos níveis de pan-lamininas, o que poderá indicar a existência de um sistema compensatório. Em relação à comunicação célula-ECM foi utilizado *Western Blot* para quantificar a ativação de STAT3, proteína responsável pela transdução de sinais extracelulares e cujo gene codificante é um conhecido oncogene. Não foram observadas diferenças na ativação de STAT3 entre esferoides WT ou *LAMA2*-KO. A técnica de PCR quantitativo (qPCR) foi também usada para determinar os níveis de expressão de dois genes de interesse (GOI) identificados na plataforma cBioPortal como estando alterados em amostras de melanoma com alterações em *LAMA2*: *MXRA5* e *MAPK6*. Não foram encontradas diferenças significativas na expressão destes genes entre esferoides de diferentes linhas celulares, apesar de *MXRA5* ter tido uma ligeira tendência para uma maior expressão em esferoides *LAMA2-KO*.

Para além do objetivo principal este projeto teve ainda como objetivo secundário estabelecer uma linha celular A375 de sobre-expressão de *LAMA2* (OE). Para o fazer foi escolhido o sistema CRISPR *activation* (CRISPRa), que permite a sobre-expressão de um gene guiando um ativador transcricional (neste caso VP64) até à zona do promotor desse gene, usando RNAs guia (gRNAs) e uma CAS9 endonuclease morta (dCAS9). gRNAs para a zona promotora do gene *LAMA2* foram definidos utilizando vários programas públicos e os plasmídeos usados para a originar a linha foram gerados pela inserção desses gRNAs num lentiSAM v2 *backbone*, através de clonagem molecular. Após confirmar a inserção correta destes gRNAs células A375 foram transfetadas e selcionadas. Para além das linhas *LAMA2*-OE foi também gerada uma linha *scramble*, que serviu de controlo. Os níveis de expressão de *LAMA2* foram verificados através de qPCR e pelo menos uma das linhas geradas teve expressão significativamente maior que a linha WT.

Por fim estas novas linhas celulares foram também utilizadas para gerar esferoides. Estes foram caracterizados em termos de crescimento e morte celular. Não foram observadas diferenças significativas em termos de crescimento ou morte celular, que tal como anteriormente não excedeu os 2%. A expressão de *MXRA5 e MAPK6* foi também avaliada, não tendo sido observadas diferenças significativas. Ainda assim a expressão de *MXRA5* aparentou ter uma ligeira tendência para aumentar nos esferoides *LAMA2*-OE. Em conjunto com a tendência anterior é possível que exista uma relação entre os níveis de *MXRA5* e *LAMA2*, sendo necessárias mais experiências para descortinar se tal relação de facto existe.

No geral este projeto foi bem-sucedido no estabelecimento de um modelo 3D para investigar o papel da ECM, e em particular *LAMA2*, na progressão tumoral. A geração de uma linha de sobre-expressão de *LAMA2* representa também um passo importante para a investigação futura do papel deste gene em melanoma e potencialmente noutros cancros e doenças. Apesar de não necessariamente significativos, os resultados preliminares obtidos, em conjunto com estas importantes ferramentas, abrem o caminho a trabalhos futuros.

Palavras-chave: Melanoma, Esferoides, *LAMA2*, Sobre-expressão, Matriz Extracelular

Contents

List of Tables

List of Figures

List of Abbreviations

2D - Two-dimensional
3D - Three-dimensional
BLAST - Basic Local Alignment Search Tool
BM - Basement membrane
BS - Blocking Solution
BSA - Bovine serum albumin
CAF - Cancer associated fibroblast
cDNA - Complementary DNA
CRISPRa - CRISPR activation
Ct - Cycle threshold
CVD - Cardiovascular disease
DABCO - 1,4-diazabicyclo[2.2.2]octane
dCas9 - Endonuclease dead Cas9
DMEM - Dulbecco's Modified Eagle's Medium
ECM - Extracellular matrix
EMT - Epithelial to mesenchymal transition
FAK - Focal adhesion kinase
FBS - Foetal bovine serum
GFP - Green Fluorescent Protein
GFP+ - GFP positive
GOI - Gene of interest
gRNA - Guide RNA
***LAMA2*-KO -** LAMA2 knockout
***LAMA2*-OE -** LAMA2 overexpression
LAMA2-CMD - LAMA2-defficient congenital muscular dystrophy
LB - Lysogeny broth
MAPK - Mitogen-activated protein kinase
MAPK6 - Mitogen-activated protein kinase 6
MMP3 - matrix metalloproteinase-3
mTOR - mammalian target of the rapamycin
MXRA5 - Matrix associated remodelling 5
NCD - Non-communicable disease
PBS - Phosphate saline buffer
PCR - Polymerase Chain Reaction
PFA - Paraformaldehyde
PI - Propidium Iodide
PI3K - phosphatidylinositol 3-kinase
P-STAT3 - STAT3 phosphorylation on tyrosine 705
PVDF - Polyvinylidene fluoride
qPCR - Quantitative PCR
RT - Room temperature
STAT3 - Signal transducer and activator of transcription 3
TBST - Tris Buffered Saline 0,1% Tween
TBSTX - Triton X100 in 1xTBST
TCGA - The Cancer Genome Atlas
UV - Ultraviolet
WT - Wild type

1. Introduction

1.1. Melanoma

In the 21st century cancer has become a major public health, societal and economical problem. It is currently the second leading cause of premature death caused by non-communicable diseases (NCDs) in most countries, with only cardiovascular disease (CVD) standing above it, which is predicted to change in the coming years[1,2].

Melanoma, a type of skin cancer, is one of the fastest growing cancers of the last few decades, being the 17th most commonly diagnosed cancer worldwide in 2022, accounting for 3.7% and 2.9% of worldwide diagnosed cancers in males and females, respectively [1,3,4]. Although it only accounts for about 4% of all skin cancers, malignant melanoma prognosis is often poor, with cutaneous melanoma (the most common kind) being responsible for 1.7% of worldwide cancer deaths (excluding other non-melanoma skin cancers) and 75% of skin cancer caused fatalities [5,6]. These rates can vary widely, depending on several factors, and notably seem to be higher in northern-hemisphere and fair-skinned populations [4,5,7–9].

Melanoma arises from genetic and epigenetic alterations in melanocytes. Melanocytes are present throughout various tissues, may display some heterogeneity and are involved in many different functions[10]. Originating in the neural crest, melanocytes go through several steps of migration, proliferation and lineage specification, before becoming mature melanocytes. The culmination of this lifecycle, and what gives them their name, is the ability to produce melanin in organelles called melanosomes. Other cell types such as the pigmented epithelium of retina, some neurons and adipocytes are also able to produce melanin [10]. Considering the different roles played by these cells, it is unlikely that melanin production is melanocytes' only function in many of the tissues where they are found. However, it seems to be the main function of melanocytes located in the basal layer of the epidermis [4–8,10–13]. Here the production of melanin is paramount since cells in the skin are routinely exposed to DNA damaging ultraviolet (UV) radiation and melanin is capable of absorbing and scattering such radiation [4–8,10–13].

The transformation of melanocytes into melanoma results from various factors, both intrinsic, like family history and genetic predisposition (5-10% of cases) and exogenous, including diet and exposure to UV radiation (which accounts for 60-70% of cases) [11]. Indeed, despite their role in protecting other cells from UV radiation, melanocytes themselves are susceptible to the DNA damaging effects of this radiation. In fact, cutaneous melanomas arising from these cells are known to carry high numbers of so called ultraviolet-signal mutations. Additionally melanin is known to produce free radicals due to its interaction with UVA radiation, adding yet another potential source of mutations and genetic aberrations to these cells due to UV exposure [7].

Considering that melanomas have one of the highest mutation loads in all cancers it is difficult to identify driver mutations in these cancers. Nevertheless, some commonly altered genes have been found. The most common is *BRAF*, an oncogene belonging to the mitogen-activated protein kinase (MAPK) pathway, that is altered in more than 50% of cases [7,13–15]. It is followed by *NRAS*, an intracellular GTPase responsible for stimulating cellular processes that include apoptosis, proliferation and differentiation. It is also part of the MAPK pathway and is altered in ~20% of melanomas [7,13–16]. Other commonly altered genes are those associated with apoptosis resistance (*TP53*), cell cycle control (*CDKN2A*), cell identity (*ARID2*), metabolism (*KIT*) and telomere maintenance (*TERT*) [7,13,14]. In addition to these genetic alterations (and often as a consequence) several signalling pathways become altered in melanoma, namely MAPK signalling pathway (associated with the regulation of proliferation, cell death and

differentiation) and the phosphatidylinositol 3-kinase (PI3K)/AKT/mammalian target of the rapamycin (mTOR) pathway (associated with cell survival, metabolism, metastasis and angiogenesis) [7,17,18].

Another important step in the progression of melanoma is the disruption of the extracellular matrix (ECM) [14].

1.2. ECM and Basement Membrane

The ECM is a complex acellular network present in all tissues. It is composed of several molecules, the most common being collagens, elastin, glycoproteins (such as fibronectin and laminins) and proteoglycans [19–23]. Traditionally it was seen as a support structure, but over the last decades it has been increasingly demonstrated that it plays a much broader role in the functioning of tissues. Besides the structural role, the ECM's functions include participating in cell-cell communication, through adhesion receptors such as integrins, as well as by serving as a reservoir and means of transport for several signalling molecules, including cytokines and growth factors [19–23]. The mechanical properties of the ECM are also fundamental in modulating cell behaviour, changing how cells proliferate and migrate [19–23].

ECMs can be classified into two distinct categories: interstitial ECM and basement membrane (BM) (**Figure 1.1**) [20,24]. The interstitial ECM fills the space between cells, being mainly produced by stromal cells [24]. It is composed of an assortment of collagens, as well as other proteins, glycoproteins and proteoglycans such as fibronectin, elastin and tenascin (**Figure 1.1**) [22,24]. It serves multiple purposes including providing structural support and modulating cell proliferation, migration and differentiation [19,22,23]. The BMs are a specialized type of ECM that surround tissues and isolate them from the stroma. They are thin, self-assembling sheets mainly composed of collagen IV and laminins. In addition to having a supportive role, BMs are fundamental for the healthy functioning of cells and tissues. They are essential in early morphogenesis, being responsible for the coordination and establishment of polarity in early cells and tissues. BMs communicate with cells via laminin-integrin interactions, controlling mechanisms such as cell migration, proliferation and tissue maintenance. Additionally, by allowing strong cell-matrix interactions BMs provide a strong barrier function, protecting cells and tissues from potential outside aggressions [19,21,25,26].

An important aspect of ECM is its dynamic nature. The ECM is in a constant state of remodelling, whether by synthesis and deposition of new matrix components, alterations in composition or by the degradation of the existing matrix[21,25]. This is a process tightly regulated by cell-matrix interactions, which occur mainly via integrins. ECM remodelling is extremely important during development, with matrices changing as tissues mature [21,25,27–31]. In adult tissues ECM remodelling is essential for tissue turnover and maintaining homeostasis, as well as wound healing. It also plays a role in regulating signalling through the release of signalling molecules [21,25,27–31].

Since ECMs play such an important role in a wide variety of cellular and tissue functions, the maintenance of their proper composition and morphology, and thus biochemical and mechanical properties, is essential in keeping tissue homeostasis. Changes in these ECM properties, through the dysregulation of the proper remodelling process, often lead to and are a consequence of disease, including cancer [20,21,23,27,30,31].

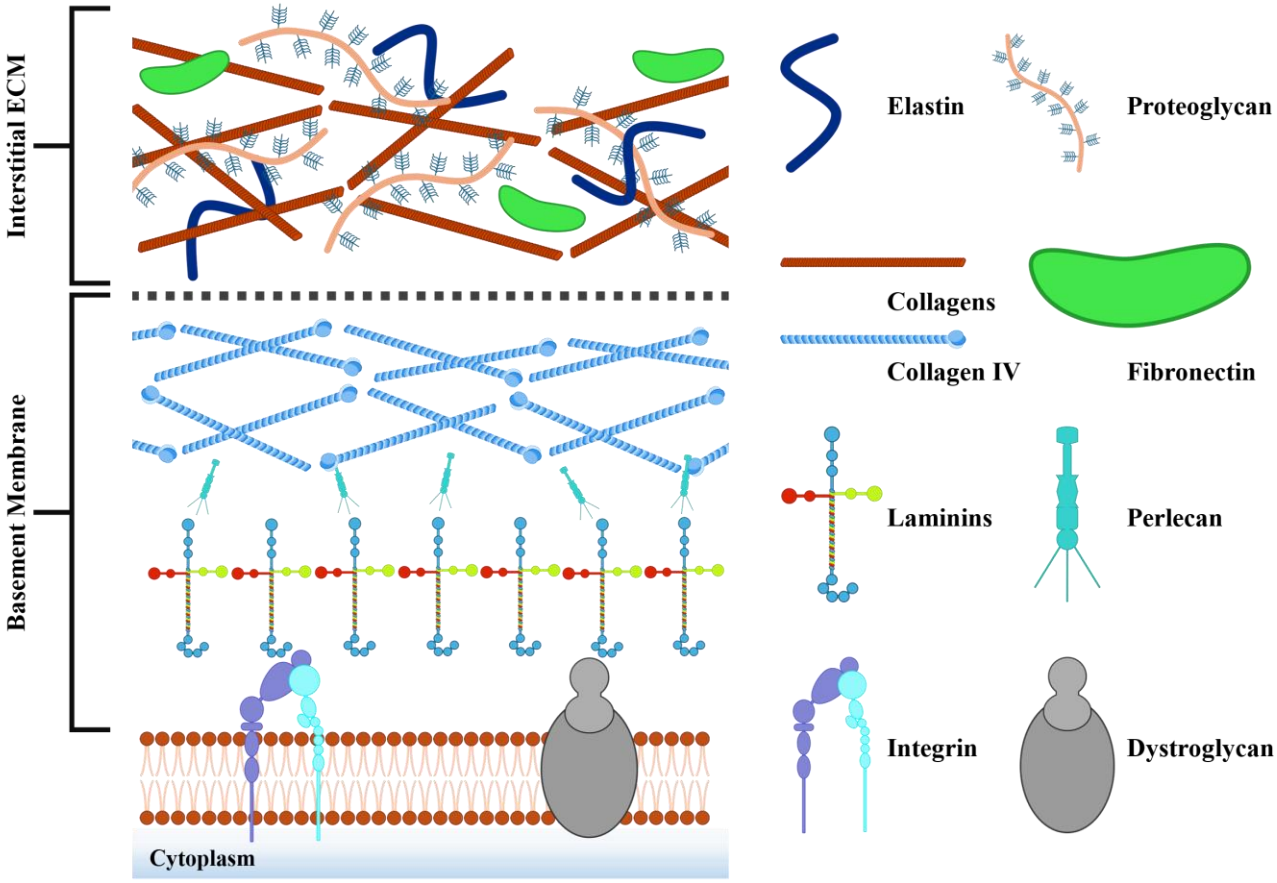

Figure 1.1 – Simplified schematic representation of the interstitial extracellular matrix (ECM) and basement membrane. ECMs can be classified into two different types: the interstitial ECM, filling the space between cells, which is mainly composed of an assortment of collagens, glycoproteins and proteoglycans such as fibronectin, elastin and tenascin; the basement membrane is thinner, isolates cells from the stroma and is mostly composed of collagen IV and laminins. Transmembrane receptors, such as integrins and dystroglycans, mediate cell-cell and cell-matrix communication. Not to scale.

1.3. ECM and Cancer

The hallmarks of cancer are a set of functional capabilities human cells acquire as they progress from normal to tumour cells. Originally proposed by Bob Weinberg and Douglas Hanahan in 2000, there have been several revisions and additions to these hallmarks over the years [32]. Following a revision in 2011, there are eight hallmarks of cancer, which have been experimentally validated by numerous laboratories: sustained proliferative signalling, evasion of growth suppressors, resistance to cell death, replicative immortality, angiogenesis, activation of invasion and metastasis, reprogramming of cellular metabolism and immune evasion [33]. In addition to these hallmarks, to better represent the intricacies of cancer, there are two enabling characteristics: genomic instability and tumour promoting inflammation [33], key features that promote tumorigenesis by promoting high mutation rate or fostering cancer cells expansion and not elimination, respectively. The latest model of the cancer hallmarks, from 2022, also proposes the inclusion of two additional emerging hallmarks (unlocking phenotypic plasticity and senescent cells) and two other enabling characteristics (non-mutational epigenetic reprogramming and polymorphic microbiomes), which have a growing body of evidences showing that they play a crucial role in tumorigenesis [34]. In addition to the hallmarks of cancer and the enabling characteristics, there are also mechanisms that act as modulators of the cancer hallmarks, such as ECM remodelling [31,35]. Considering the involvement of the ECM in the processes that govern and regulate many of these cancer hallmarks

it should not be surprising that ECM alterations are a common feature in various cancers, with many displaying abnormal matrices, as both a consequence and driver of tumour progression, by enabling these cancer hallmarks [36].

Excess deposition of matrix components, for instance, may lead to increased stiffness, a characteristic of solid tumours [20,22,23,36]. Increased rigidity enables sustained proliferative signalling, apoptosis resistance and replicative immortality, as well as neovascularization. It also promotes cell migration leading to an increased metastatic potential in these tumours. This can happen directly by an increase in integrin dependent cell adhesion or indirectly due to a compromise in vascular integrity leading to higher extravasation potential [36]. Strong adhesion to the matrix can also reduce the effectiveness of tumour suppressing mechanisms, for example by reducing p21 and p15 expression, allowing cancer cells to evade these growth suppressors [36]. On the other hand, abnormal matrix remodelling can result in a reduction or loss of matrix components. This can lead to thinning of the BM, which enhances the invasive potential of cancers, which typically must breach this barrier to invade tissues [36]. Additionally the ECM can also directly and indirectly impede immune response, as well as contribute to the deregulation of metabolism by promoting the activation of glycolysis increasing pathways, such as the PI3K pathway [36].

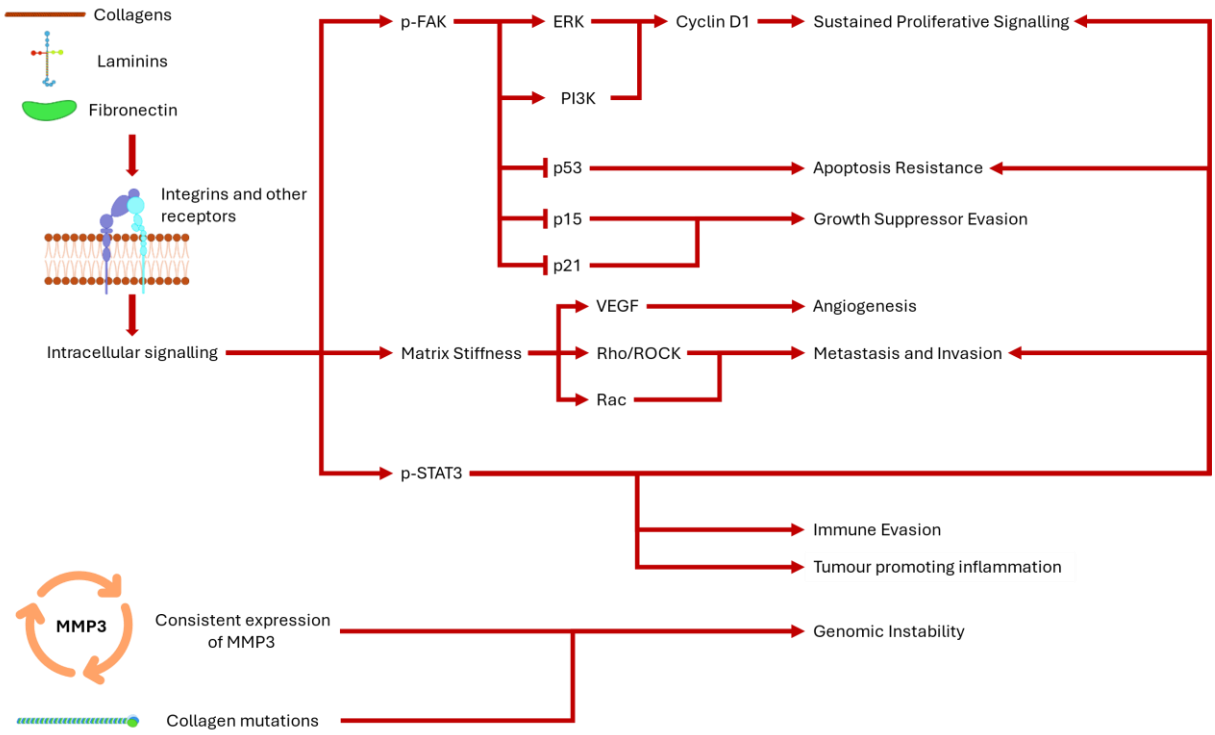

Figure 1.2 – Simplified summary showing examples of the role of the ECM in some hallmarks of cancer and enabling characteristics. Several ECM molecules can interact with integrins and other receptors which in turn activate intracellular signalling. This signalling can lead to the activation of several other signalling cascades and even modulate properties of the ECM such as stiffness. These all contribute to the modulation of various cancer hallmarks and enabling characteristics. Other alterations in ECM components, such as collagen mutations and consistent expression of matrix metalloproteinase-3 (MMP3), can lead to genomic instability which in turn contributes to the appearance and progression of tumours.

Certain ECM alterations also serve as an enabler for disease onset. An abnormal ECM can increase genomic instability, with inherited mutations in collagen components known to elevate the risk of smooth muscle tumours and skin cancer [36]. Chronically inflamed tissues, known to be at a higher risk of malignant transformation, are also a result of altered ECMs [36].

A fundamental part in how the ECM contributes and controls these cancer hallmarks and enabling characteristics is its interaction with intracellular signalling pathways. Focal adhesion kinase (FAK) and signal transducer and activator of transcription 3 (STAT3) are two notable examples of proteins involved in these signalling pathways also known to play a major role in tumour progression [36–38]. FAK mediates integrin signalling in focal adhesion sites and has been shown to have increased levels in several cancers [36,37,39,40]. It plays a significant role in modulating various cancer hallmarks, like sustained proliferative signalling, apoptosis resistance and growth suppressor evasion [36,37,39,40]. STAT3 is responsible for the transduction of extracellular signals into transcriptional changes [38,41]. Thus, it regulates many crucial processes such as cell growth, survival, differentiation, regeneration, immune response and cellular respiration [38,41]. Because of this its involvement in tumour progression and cancer should come as no surprise. In fact, *STAT3* is a well-known oncogene (altered in ~70% of cancers), with its constitutive activation (via phosphorylation of its tyrosine-705 (Y705)) being associated with the transformation of normal cells into tumour cells, resistance to cell death and increased metastatic potential, as well as the induction of tumour-promoting inflammation and immune evasion [38,41–43].

1.4. *LAMA2* role in cancer

As previously mentioned, one of the main components of the BM, along with collagen, are laminins. Laminins are large heterotrimeric glycoproteins composed of one α, one β and one γ chains [44,45]. In mammals there are five α chains, four β chains and three γ chains variations. These chains combine into a cross-shaped heterotrimer to form different laminin isoforms, identified by the number of each chain. For example, laminin-111 is composed of one each of the α1, β1 and γ1 chains. Laminins are essential in the assembly of BMs, as well as their structural integrity through their interaction with collagen [25,46]. They also serve as important mediators of cell-matrix interactions, providing binding sites for integrin, a key regulator of cell-cell and cell-matrix interactions [46].

Due to these important roles, alterations in these proteins are often associated with disease. One example of this is *LAMA2* congenital muscular dystrophy (LAMA2-CMD). In this disease defects in the α2 chain of laminins-211 and 221, caused by mutations in the *LAMA2* gene, lead to severe weakening of the muscle and hypotonia, and eventually compromises a patient's ability to walk, stand, swallow and breathe [47,48].

Although muscular dystrophies are some of the more common and well characterized diseases linked to mutations in ECM or ECM-related components, these proteins are also known to play a role in several cancers [49]. For instance laminin-322 is known to have altered expression in cancer associated fibroblasts (CAFs), tumour cells and the tumour microenvironment, which leads to increased invasion [26,45]. Laminin-111 is known to increase tumour growth, proliferation and apoptosis resistance in some cancer cells [26,50].

LAMA2 specifically is also known to play a role in various cancers [49]. Mutations in this gene are found in inflammatory breast cancer [51], laryngopharyngeal squamous cell carcinoma [52] and hepatocellular carcinoma [53]. *LAMA2* is also differentially expressed in ovarian cancer [54] and to be a driver of DNA methylation in pituitary adenoma [55]. It has also been found that laminin-α2 can regulate cell proliferation, apoptosis resistance and invasion potential in breast cancer through the MAPK signalling pathway [56].

All of this indicates that laminin-α2, laminins and the BM in general likely have an important role in regulating tumour progression. One way in which this role can potentially be dissected is by using *in vitro* models.

1.5. *In vitro* models to dissect the role of BM in cancer

Considering the complexity of cancer, establishing models that at the same time can both simplify but also mimic tumours and their environments is of extreme usefulness. *In vitro* biological models have been a staple of biological research for decades. These models have been at the centre of many discoveries and have been used to understand a large number of biological functions and mechanisms, both in homeostasis and disease [57–59].

Monolayer, two dimensional (2D), cell cultures have been one of the most used *in vitro* models [58,60]. As the name suggests, these consist of cells cultured as a single layer in a flat surface. Part of the reason this type of model has been so ubiquitous is its simplicity and convenience. Several pieces of evidence, regarding the hallmarks of cancer, such as cell proliferation, DNA damage mechanisms and genomic instability, have been gathered using such systems, and they have been regularly used to test susceptibility to chemotherapeutic agents [60–62]. Despite this extensive use, there are many aspects in which monolayer cell cultures fail to accurately represent the *in vivo* condition [57,58]. For instance, cells cultured in 2D conditions often have altered biological functions, with proliferation, apoptosis, metabolism, transcriptional regulation and receptor expression all being in some way different to the *in vivo* condition [58,60]. These differences can and do impact the predictive power of results obtained using these models [58,60]. In fact, the validity of drug tests using 2D cultures is a well-known problem, with drugs eliciting different reactions *in vivo* than what was expected by *in vitro* testing [58,60].

All of these issues are a result of forcing cells to grow on a flat surface, unlike what happens in the living organism [58,60]. This mode of growth limits cell-cell interactions and outright prevents the establishment of an ECM and consequently these models lack cell-matrix interactions [57–60,63,64]. As such, 2D cultures fall short on providing an accurate representation of the ECM and are suboptimal for research involving the role of this structure [58,60]. In contrast, three-dimensional (3D) models, by allowing cells to grow in a 3D environment with a larger number of cell-cell and cell-matrix interactions, are known to be better than classic monolayer cultures at simulating many *in vivo* mechanics, especially when it comes to ECM properties [57–59,63,64].

Spheroids are a type of 3D model in which cells are grown in free-floating aggregates [58,65]. Because they are a 3D structure cell-cell interactions are more numerous and there is a pH, nutrient and oxygen gradient between the outer and inner regions of the spheroids, mimicking the *in vivo* tumour microenvironment [64,65]. They are also known to produce their own ECM, allowing for cell-matrix interactions and have been shown to have gene expression profiles closer to patient tumours, relative to 2D cultures [65]. All of this makes spheroids overall better at mimicking *in vivo* tumours than 2D cultures. For this reason, they have been regularly used to explore aspects related to cancer, including response to drug and radiation treatments [65,66], migration [67,68] and invasion [67,69].

All in all, when attempting to dissect the role of the ECM and its components, the use of 3D models is likely to prove advantageous, not only in providing potentially more accurate results but also in reducing the use of animals used in experiments, thus respecting the 3R rules [70]. Furthermore, spheroids seem to be a good choice of 3D model, considering they are known to produce their own ECM and are relatively cheap [64].

1.6. Aims of the Project

Considering the importance of ECM as a key modulator of the hallmarks of cancer and enabling characteristics, the aim of this project was to establish *in vitro* 3D cancer models to study the impact of ECM in tumour progression. Specifically, how alterations in *LAMA2* affect tumour progression. Human melanoma A375 WT and *LAMA2*-knockout (KO) cell lines were used to test the generation of spheroids, a type of *in vitro* 3D model, using two different methods. After determining the best method and

establishing the protocol for the successful generation of spheroids, they were characterized in terms of growth, cell proliferation and death, gene expression and protein alterations by using various techniques, including qPCR, immunofluorescence, flow cytometry and resazurin assay. This characterization will serve as a preliminary look into the effect of *LAMA2* absence in tumour progression and as a way to test the use of these techniques in spheroids, for future use.

In addition to this main goal another aim of this project was the establishment of A375 *LAMA2* overexpression (OE) cell lines using the CRISPR Activation (CRISPRa) technology, to further expand the tools available to study the impact of *LAMA2* in tumour progression and disease.

Overall, this project provides a framework to use 3D *in vitro* models to study the role of ECM and *LAMA2* in tumour progression, building upon the work already done in the host lab.

2. Materials and Methods

2.1. 2D Cell Culture

2.1.1. Cell culture

Human A375 wild type (WT) and *LAMA2* knockout (KO) (previously generated in the host laboratory [71]) melanoma cell lines were maintained in Dulbecco's Modified Eagle Medium (DMEM) supplemented with 10% Foetal Bovine Serum (FBS) and 1% Penicillin and Streptomycin (100 – 120 U/mL of penicillin and 0.1-0.12 mg/mL of streptomycin). They were kept in an incubator at 37 ºC, 5% CO_2 and constant humidity. They were passaged regularly, when confluency reached approximately 70%, using trypsin-EDTA.

2.1.2. Transfection

For transfection approximately 300 000 A375 cells were plated onto 24-well plates. After 24h growing in the conditions described in 2.1.1 they were transfected with either Lipofectamine 3000 or Fectovir, according to the manufacturer's instructions. A375 cells were transfected with OEA1, OEA2, OEA3 and scramble plasmids, generated by cloning the gRNAs on **Table S1** onto a lentiSAM v2 (Puro) (Addgene plasmid #92062) backbone (**Figure S1**). Efficiency of transfection was monitored through the co-transfection with a GFP plasmid (Addgene plasmid #105530), under a fluorescence microscope (Optika IM-3LD4).

2.2. 3D Cell Culture

2.2.1. Spheroid Generation

Spheroids were generated using A375 cell lines and maintained in DMEM supplemented with 10% FBS and 1% Penicillin and Streptomycin (complete medium) and kept in an incubator at 37 ºC, 5% CO2 and constant humidity. Two different methods were employed, agarose-coated wells and hanging drops. For each method cells were counted using a Neubauer chamber to determine the number of cells in the initial cell culture and subsequently the concentration was adjusted.

2.2.1.1. Hanging Drops

To generate spheroids using the Hanging Drops method 20 μL drops of a cell suspension with $5x10^5$ cells/mL of concentration (10000 total cells per drop) were placed on the lid of a 10 cm Petri dish, in a 6x6 matrix. The lid was then inverted and placed on top of the dish. Petri dishes with drops were placed on an orbital shaker for 10 minutes to facilitate cell aggregation. Afterwards the bottom part of each dish was filled with 10 to 15 mL of PBS, to prevent dehydration and left to incubate for 3-4 days. After this incubation period spheroids were transferred to wells of a 96-well plate, previously coated in 1% agarose to prevent cells from adhering to the bottom of the wells. Then, 100 μL of DMEM complete medium were added to each well. Whenever necessary medium was changed.

2.2.1.2. Agarose Plate

Agarose Plate spheroids were generated by placing 20 μL of a cell suspension with $5x10^5$ cells/mL of concentration (10000 total cells per drop) in wells of a 96-well plate previously covered with 1% agarose in 1xPBS, which prevents cell adhesion to the bottom of the well and thus promotes their aggregation into spheroids. A further 80 μL of DMEM complete medium were added to each well. Plates were placed on an orbital shaker for 10 minutes to potentiate cell aggregation and then left to incubate for 3-4 days. After this time spheroids were monitored and medium changed whenever needed.

2.3. Cell Viability Assays

2.3.1. Resazurin Proliferation Assay

Proliferation in spheroids was evaluated using the resazurin proliferation assay. This non-fluorescent compound is reduced by metabolically active cells into resorufin, which is highly fluorescent. When excited with 571 nm wavelength it emits fluorescence in the 583 nm wavelength. Since only metabolically active cells produce the fluorescent compound, their number will be proportional to the level of fluorescence. By performing the assay and measuring fluorescence over multiple timepoints this assay can be used as an indirect measure of cell proliferation. To perform the assay a 10 mg/mL resazurin solution was diluted in DMEM complete medium to obtain a 20 μg/mL resazurin solution in DMEM. Then, 100 μL of this solution were added to wells of 96-well plates with spheroids, already containing 100 μL of medium (making resazurin concentration 10 μg/mL). Spheroids were then left to incubate for 4 hours. After incubation 150 μL of the resazurin medium were transferred into a reading plate, avoiding forming bubbles. The fluorescence of this medium was measured using a Victor 3V plate reader (Perkin Elmer), by exciting it with 571 nm and measuring the emission of 583 nm (the excitation and emission peaks of resorufin). One well containing only media and incubated in the absence of spheroids was used as blank. To analyse proliferation, sets of spheroids were measured on days 3, 4, 5 and 6 post seeding and all values were then normalized to the average of measurements in the first timepoint.

2.3.2. Propidium Iodide Viability Assay

To evaluate cell viability 100uL of a 1μg/mL solution of Propidium Iodide in DMEM was added to spheroids in agarose-coated 96-well plates. Spheroids were already in 100uL of DMEM, making the final concentration 0.5 μg/mL. This compound is only permeable to dead cells, which will fluoresce with an emission peak of 618 nm when excited with 450-580 nm. Spheroids were incubated in this solution for 15 minutes and then either observed under a fluorescence microscope (Optika IM-3LD4) or dissociated, via mechanical action, and collected for flow cytometry. Flow cytometry analysis was

performed using the CytoFLEX™Flow Cytometer (Beckman Coulter) and the obtained data was analysed using the Flowjo_v10.9.0 software.

2.3.3. Spheroid Immunofluorescence

To perform immunofluorescence in spheroids they were first collected, washed with 1xPBS and then fixed with 4% paraformaldehyde (PFA) for 15 minutes. PFA was then taken out and replaced with 150 µL of 1xPBS for 10 minutes. Then spheroids were washed with 0.5% TBSTX (0.5% Triton X100 in 1xTBST) for 5 minutes, with agitation, to permeabilize cell membranes. Blocking was done by substituting the 0.5% TBSTX with a Blocking Solution (BS) (2% BSA in 0.1% TBSTX) for 1h. After permeabilization spheroids were transferred to 50 µL drops of the primary antibodies and left to incubate overnight at 4ºC. The next day they were washed with 0.1% TBSTX (0.1% Triton X100 in 1xTBST) and then incubated in 50 µL drops containing both the secondary antibody and methyl green (1:150), for nuclear staining, overnight at 4ºC.

Spheroids were mounted between two 40x60mm coverslips, in 40-80 µL of Mowiol-DABCO (2.4g of Mowiol, 4.8 mL of 100% glycerol and 2.5% DABCO in H_2O; pH 8.5) mounting media. To prevent spheroids from being flattened thin strips of plasticine were used as spacers between the two coverslips. Images were captured on a Leica SP5 confocal microscope and analysed using ImageJ 1.54f. This protocol was adapted from Bergdof *et al.* (2021) [72].

A list of the used antibodies and solutions can be found on **Tables S2** and **S3**, respectively.

2.4. Molecular Biology

2.4.1. RNA extraction, cDNA and qPCR

Cells were collected in microcentrifuge tubes, centrifuged and washed with 1xPBS. The resulting pellet was lysed in 500 µL of Triple Xtractorl™ reagent to dissociate nucleoprotein complexes. Chloroform was added to the solution, the tube was vortexed and then it was left standing for 3 min to allow phase separation. Solution was then centrifuged to better separate the aqueous phase, containing the RNA, from the other phases. This phase was transferred into a new tube. Then, 250 µL of isopropanol were added to this new tube to precipitate the RNA. After another centrifugation the supernatant was discarded and the pellet washed twice with 75% ethanol. After washing, ethanol was removed and the pellets left to air dry. To solubilize the RNA 20 µL of RNAse free water were added to the pellet and it was incubated in a thermoblock at 55 ºC for 10 minutes. RNA was quantified using a NanoDrop One and then stored at -20 ºC until further use.

Complementary DNA (cDNA) was synthesized from the previously extracted RNA using the Xpert cDNA Synthesis Kit (#GK80.0100). For each sample the reaction mixture was made with the following components: 4 µL 5× reaction Buffer, 1 µL dNTP mix, 1 µL random hexaprimers, 1 µg of extracted RNA, 1 µL Xpert RTase with RNAse inhibitor (200 U/µL) and RNAse free water up to 20 µL total reaction volume. The reaction was briefly centrifuged and placed in a thermocycler at 25 ºC for 10 min, 55 ºC for 50 min and 85 ºC for 5 min. The obtained cDNA was stored at -20 ºC until further use.

For quantitative PCR (qPCR), a reaction mixture with 10 µL of total volume was set up with the following components, per well: 5 µL of Xpert Fast SYBR, 0.4 µL of forward and 0.4 µL of reverse primer oligos (**Table S4**) and 3.2 µL of RNAse Free water. The mixture was then distributed into the wells of a 96-well plate and 1-2 µL of cDNA were added to each well. Each sample was run in duplicate. The plate was sealed with an optically transparent film, protected from light and centrifuged, before performing the qPCR reaction in a CFX96TM Real-Time PCR Detection System (Bio-Rad). The qPCR protocol can be found on **Table S5**.

For qPCR analysis, the threshold cycle (Ct) values of the gene of interest (GOI) and the housekeeping gene were compared, according to the equations below (2.1, 2.2). The quality of all qPCR reactions was assessed by melting curve analysis.

(2.1) ΔCt = Ct (GOI) - Ct (housekeeping)

(2.2) Fold difference to housekeeping = $2^{-\Delta Ct}$

2.4.2. PCR and Purification

For PCR analysis of *LAMA2* promotor region, cell pellets were lysed in 75 µL of a 25 mM NaOH/0.2 mM EDTA lysis buffer and then placed on thermocycler for an 30min at 95 ºC. After this time, samples were cooled to 4ºC and 75 µL of a 0.40 mM Tris HCl (pH 5.5) solution were added to the samples. They were then centrifuged at 4000 rpm for 3 minutes. PCR was performed using 1 µL of the obtained DNA and Q5 High Fidelity 2X Master Mix (New England Biolabs), according to the manufacturer's instructions. Primers and PCR protocol can be found on tables S6 and S7. Part of the PCR reaction was loaded onto a 1.5% agarose gel stained with Red Safe to visualize the efficiency of the reaction. The remainder was purified using the Promega Wizard® SV Gel and PCR Clean-Up System, following the manufacturer's instructions and then sent for Sanger sequencing (YouTube It service, StabVida).

2.4.3. Molecular cloning

To construct the *LAMA2* overexpression and scramble plasmids, the forward and reverse oligonucleotide pairs found in **Table S1** were cloned into a lentiSAM v2 (Addgene plasmid #92062) backbone (**Figure S1**).

The LentisamV2 plasmid was digested with BsmbI-v2 restriction enzyme for 1h at 37 ºC and dephosphorylated for another hour with alkaline phosphatase. The linearization of the plasmid was confirmed by gel electrophoresis and the resulting linearized plasmid was gel purified and quantified using NanoDrop One. Each oligo pair was annealed by adding 0.5 µL of each (forward and reverse) to an annealing buffer containing 10X T4 Ligation buffer, 0.5 µL PNK and 6.5 µL dH_2O and placing this mixture in a thermocycler at 37 ºC for 30 min followed by 5 min at 95 ºC and then gradually decreasing the temperature to 25 ºC by 5ºC every minute. To ligate the annealed oligos and the LentisamV2 linearized backbone, 1 µL of a 1:100 dilution of the obtained oligo duplexes was added to 5.9 µL dH2O together with 1 µL of the previously linearized plasmid, 1 µL of T4 ligase and 1.1 µL of T4 ligase buffer. This ligation reaction was done at room temperature (RT) for 30 minutes.

Chemically competent *Escherichia coli* were transformed with either the plasmids from the ligation reaction or the linearized LentisamV2 plasmid (as a control). These bacteria were then plated on lysogeny broth (LB) agar plates containing 100 µg/mL of ampicillin and left to grow overnight at 37 ºC. Colony PCR was performed on ampicillin resistant colonies using the sequencing primer (pX330_U6_seq_fwd [73], **Table S8**) and the corresponding reverse oligo for each plasmid, to confirm the presence of the oligo in the correct orientation (colony PCR protocol on **Table S9**). Colonies confirmed to be successfully transformed were grown overnight at 37 ºC with agitation in LB broth. A fraction of each culture was used to create stocks in 50% glycerol and the remaining culture to purify plasmid DNA with a plasmid purification kit (GRiSP) according to the manufacturer's instructions.

The correct cloning of the gRNA sequences into the purified plasmids was confirmed via Sanger sequencing (StabVida, Portugal).

2.4.4. Western blot

2.4.4.1. Protein Extraction

To extract protein cells (once at ~70% confluence) and spheroids (20 spheroids per line) were pelleted and suspended in 200 µL of SDS-PAGE (20% Glycerol, 4% SDS 100mM, Tris pH 6.8, 0.2% Bromophenol blue, and 100 mM DTT). They were then homogenized using a Retsch MM400 Tissue Lyser to shred DNA and RNA. The obtained lysates were heated at 70 ºC for 10 minutes and then centrifuged at 4ºC and maximum speed for 5 minutes. The supernatant was transferred to a new microcentrifuge tube and protein concentration was determined by the ratio of 260 nm to 280 nm absorbance using a NanoDrop One. Samples were stored at -20 ºC until use.

2.4.4.2. Western Blot

Proteins were separated using a 10% polyacrylamide gel. Around 70-100 µg of each sample were loaded into each well and ran in 1x Running Buffer (3.02 g Tris base, 14.42 g Glycine, 1 g SDS in 1 L distilled water) at 150 V for 1h-1h30min, using the Mini-PROTEAN® Tetra electrophoresis system (Bio-Rad). Proteins were transferred to a methanol activated polyvinylidene fluoride (PVDF) membrane using the Mini Trans-Blot® Cell (Bio-Rad) with chilled transfer buffer (5.82 g Tris, 2.93 g glycine in 1 L distilled water) at 100 V for 45 min. Membranes were blocked for 1h at RT in 5% powdered milk in TBST with agitation. After blocking membranes were rinsed three times, for 5 minutes, with TBST and incubated in primary antibody (diluted in 2% BSA in TBST and 0.02% Sodium Azide) at 4 ºC overnight, with agitation. The following day membranes were washed with TBST for 5 minutes and incubated with secondary antibody (diluted in 5% powdered milk in TBST) for 1h at RT. Then membranes were washed three times with TBST for 10 minutes. Chemiluminescence was detected using SupersignalTM West Pico Chemiluminescent Substrate HRP (ThermoFisher Scientific). Images were acquired using the Amersham Imager 680 RGB (GE Healthcare) and the densitometry analysis was performed using ImageJ 1.54f.

The used antibodies and dilutions can be found on **Table S2**.

2.5. Bioinformatic

2.5.1. Guide RNA and Primer design

Guide RNAs for the generation of an overexpression line using Crispr Activation were designed using online tools, namely CHOP-CHOP, CRISPR-ERA and CRISPick. Best gRNAs of each were chosen to be tested. A scramble gRNA, to serve as a control, was selected from Papes *et al.* (2022) [74]. The list of gRNAs can be found on **Table S1**.

2.5.2. Spheroid Area Measurement

A custom ImageJ script was used to automatically segment spheroids in photos and measure their area. **Figure S2** shows the script pipeline.

Stitching using the plugin based on Preibisch *et al.* (2009) was used when spheroids were too big to be captured in a single photo [75].

2.5.3. Statistical Analysis

Statistical analysis was performed using GraphPad 8.0.2. A Two-Way ANOVA with Tukey's Multiple Comparison test was used to compare the growth/area of spheroids of different A375 cell lines. To compare *LAMA2* two expression levels the One-Way ANOVA with Dunnett's multiple comparison test was used. A Two-Way ANOVA with Sidak's multiple comparison was used to compare other qPCR expression levels.

3. Results

3.1. Identifying frequency of alteration of *LAMA2* in cancer

Considering the importance of the BM in cancer and how critical laminins are to its structure and maintenance, understanding if and what laminins are commonly altered in melanoma is an important step in starting to unveil their role in this disease.

To that end, cBioPortal, an online repository of data of various cancer studies, was utilized to check which laminins were commonly altered in melanoma, by determining the frequency of genomic alterations in the five different laminin α-chains (*LAMA1-5*) in melanoma samples (**Figure 3.1**). *LAMA2* was found to be the most altered laminin α-chain in melanoma, altered in more than 25% of patient samples. Moreover, by analysing the frequency of alteration in *LAMA2* for all cancer types, *LAMA2* was found to be altered in 25% of the analysed melanoma samples, making it the top cancer type for *LAMA2* alterations (**Figure 3.1**) [76–79].

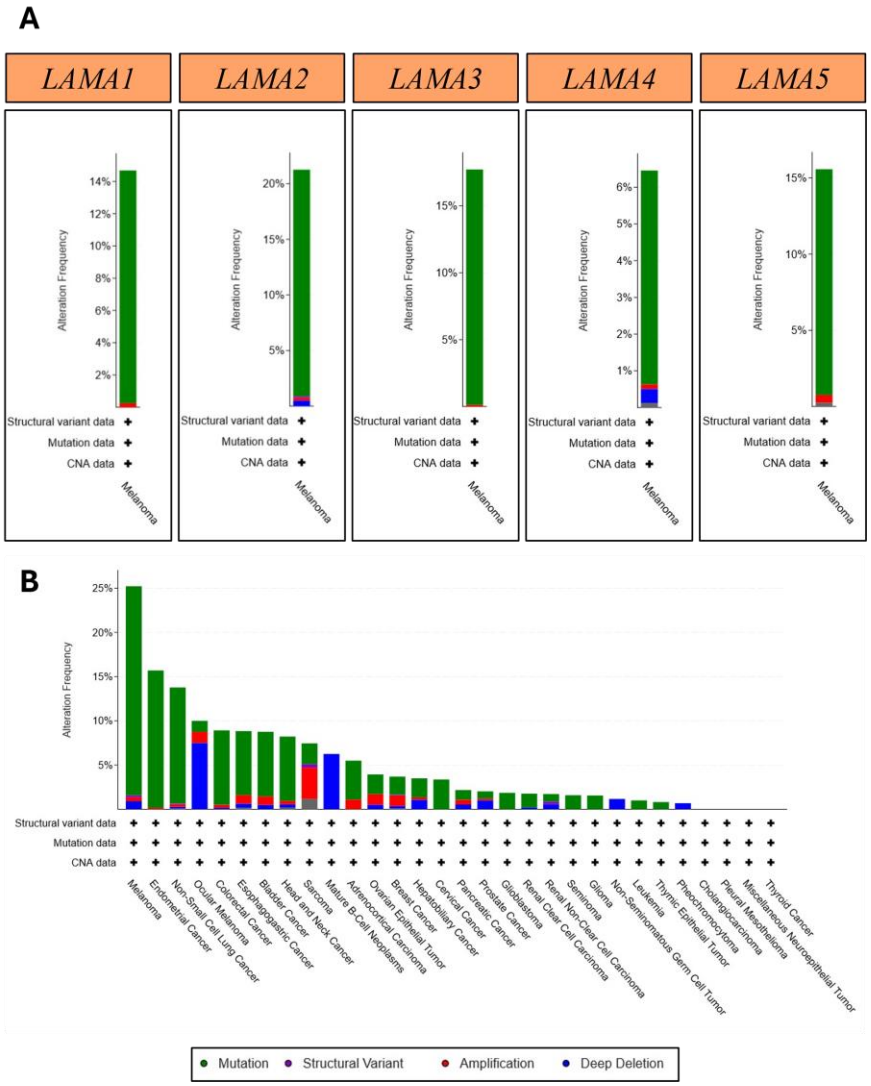

Figure 3.1 – Alteration frequency of laminins in melanoma and *LAMA2* alteration frequency in various cancers. cBioPortal was used to identify the alteration frequency of: **(A)** *LAMA1-5* in melanoma samples from the curated The Cancer Genome Atlas (TCGA) database. Data includes 1 study, 363 patients and 363 samples **(B)** *LAMA2* in several cancer types. The presented data was obtained from the TCGA database and includes 32 studies, 10953 patients and 10567 samples. The graph shows the alteration frequency of *LAMA2* in 30 cancer types. CNA – copy number alteration.

Next cBioPortal was used to compare melanoma samples with and without alterations in *LAMA2*. Several genes were found to be significantly altered when *LAMA2* is also altered, 2886 to be precise. This list was then run through the Matrisome Analyzer online tool to identify ECM and ECM related genes on the list [80]. The top 10 GOIs found through this analysis can be found on **Table 3.1**. From this list, *MXRA5*, the top gene, stands out as especially interesting considering its role in matrix remodelling, signalling and previous associations with tumour progression [81–83].

These analyses were all performed on the TCGA and PanCancer Atlas databases, since these datasets are subject to more scrutiny and so their data is expected to be more consistent and of higher quality [76–79].

Table 3.1 – Top 10 Significantly Altered ECM genes in melanoma, when *LAMA2* is altered

Top 10 Significantly Altered Core Matrissome Genes when *LAMA2* is altered in Melanoma	
1 *MXRA5*	matrix remodeling associated 5
2 *COL24A1*	collagen type XXIV alpha 1 chain
3 *SVEP1*	sushi, von Willebrand factor type A, EGF and pentraxin domain containing 1
4 *COL11A1*	collagen type XI alpha 1 chain
5 *VCAN*	versican
6 *COL6A2*	collagen type VI alpha 2 chain
7 *THBS1*	thrombospondin 1
8 *TNN*	tenascin N
9 *NTN4*	netrin 4
10 *FBN2*	fibrillin 2

3.2. Establishment of *LAMA2* overexpression cell line

Considering the data obtained through cBioPortal analysis, generating models to explore the role of laminin-α2 in melanoma is of extreme importance. To do so the goal was to compare melanoma cell lines either lacking or overexpressing *LAMA2*. Although A375 *LAMA2*-KO lines were previously established in the laboratory [71] *LAMA2*-OE cell lines were not yet available, so there was a need to first establish this type of cell line.

For that, the CRISPR Activation (CRISPRa) technology was chosen. This method works by using a construct where an endonuclease dead Cas9 (dCas9) is fused with a transcriptional activation domain (in this case VP64, which encodes a tetrameric repeat derived from human herpes simplex virus) [84–86]. Even though, the dCas9 is no longer able to cut the double stranded DNA, as is the case with the more commonly used CRISPR-Cas9 systems, it will still be directed towards a specific site by a guide RNA (gRNA) [84,85]. This site is, ideally, in the promoter region of the gene that is to be overexpressed, as the dCas9 will bring with it the transcriptional activator, allowing the overexpression of the gene [84,85].

The gRNAs for the CRISPRa based overexpression of *LAMA2* were designed using various publicly available software, as described in the Material and Methods section. An additional gRNA, dubbed scramble, was chosen from literature [74]. This scramble gRNA should not target any region of the human genome and was used to generate a control cell line for the *LAMA2* overexpression cell lines.

To verify the exact sequence of the *LAMA2* promoter regions targeted by the chosen gRNAs, and ensure that these did not present mutations, which could impair gRNA annealing and thus compromise the effectiveness of overexpression, DNA was obtained from A375 WT cells. The target regions were then amplified via PCR (primers and PCR protocol on tables S5 and S7, respectively). After confirming the success of this amplification with gel electrophoresis the PCR products were purified and sequenced by Sanger sequencing. All 3 gRNAs were found in the promoter region of the human *LAMA2* gene without mutations (**Figure 3.2A**). The sequenced region (Query) was perfectly aligned with the

reference *LAMA2* promoter region (Sbjct), except for some gaps at the beginning of the sequence, which are expected due to the low-quality base calling in the beginning of the sequence (**Figure 3.2B**). This can be further verified by observing the chromatogram and quality scores (**Figure 3.2A**).

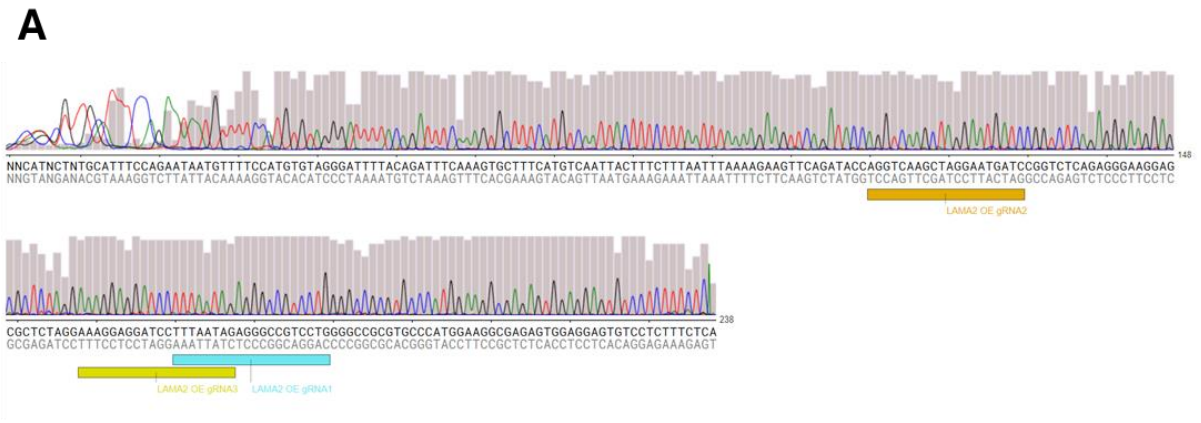

Figure 3.2 – Sequencing results of the *LAMA2* promoter region in A375 cells. The *LAMA2* promoter region of A375 cells was sequenced by Sanger sequencing to verify that the gRNAs chosen for the *LAMA2* overexpression plasmid would target the region in these cells. **(A)** All gRNA targeted sequences were found to be in this region with no mutations **(B)** Basic Local Alignment Search Tool (BLAST) was used to compare the sequenced *LAMA2* promoter region (Query) to the human reference genome (GRCh38.p14) (Sbjct).

After this confirmation, gRNAs were cloned in a lentiSAM v2 backbone via restriction enzyme-based cloning. The successful cloning for each CRISPRa gRNA and scramble was confirmed via Sanger sequencing (**Figure 3.3**).

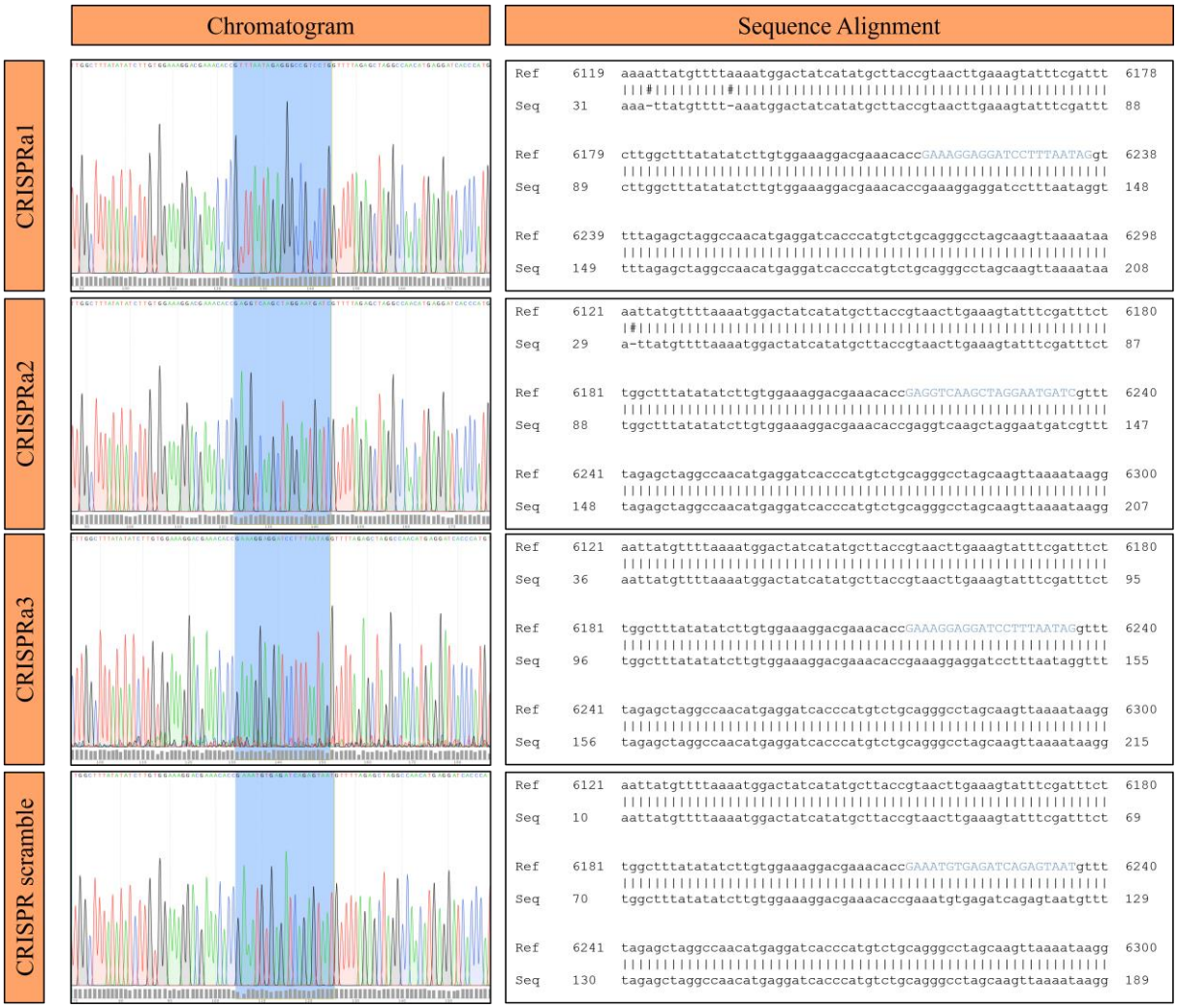

Figure 3.3 – Sanger sequencing results for CRISPRa and Scramble plasmids. The plasmids with the desired gRNA inserted by molecular cloning were Sanger sequenced to ensure it was inserted in the expected position. On the left is the chromatogram showing the base calling quality of the sequencing. On the right is the alignment of the expected sequence (Ref) and the sequenced region (Seq). The inserted gRNAs are highlighted in the chromatograms, in blue, and in cyan and uppercase in the expected sequence. | - aligned bases; # - misaligned bases.

With the successful generation of *LAMA2* CRISPRa plasmids, before the establishment of A375 cell lines overexpressing *LAMA2*, several steps in the transfection process were optimized. First, to choose a transfection method, the transfection efficiency of A375 cells using two different cationic transfection reagents, Fectovir and Lipofectamine 3000, was tested by transfecting cells with a GFP plasmid. Fectovir appeared to be more efficient, in addition to being cheaper and simpler to use, so it was used in all future transfections (**Figure 3.4A**). Transfection efficiency with Fectovir was also quantified by flow cytometry. To do this A375 WT cells were transfected with a GFP plasmid and then flow cytometry was used to quantify the percentage of GFP positive (GFP+) and therefore successfully transfected cells. Transfection was efficient with 18-25% of cells found to be transfected (**Figure 3.4B**).

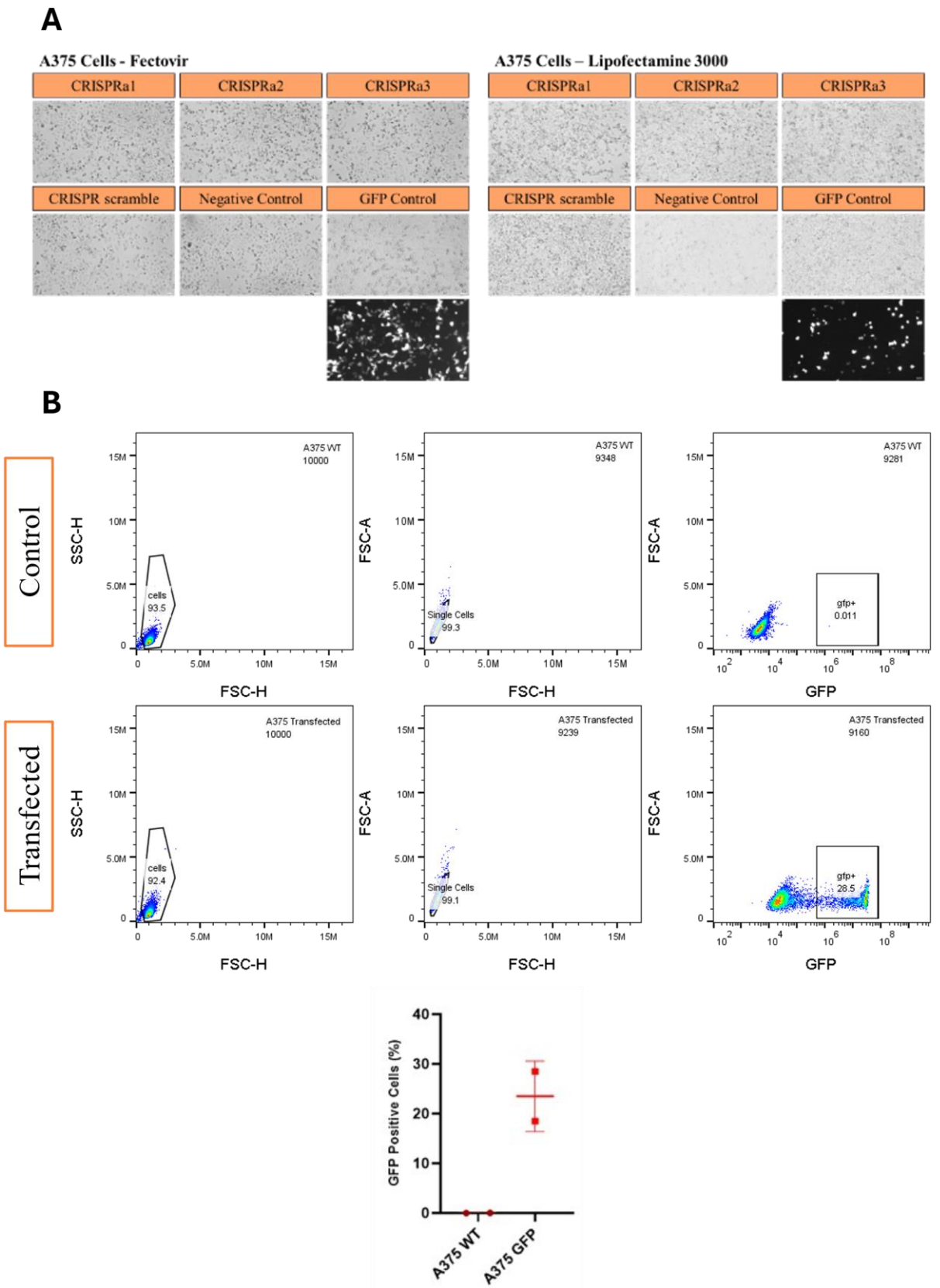

Figure 3.4 – Transfection optimization of A375 melanoma cells. (A) Efficiency of Fectovir *vs* Lipofectamine 3000 in A375 transfection. A375 cells were transfected with the *LAMA2*-OE plasmids as well as a GFP plasmid to track the efficiency of transfection**.** Cells were compared under a fluorescence microscope (Optika IM-3LD4). **(B)** To evaluate the transfection efficiency of Fectovir in A375 melanoma cells, A375 WT cells were transfected with a GFP plasmid. Flow cytometry was then used to count GFP+ to determine the percentage of successfully transfected cells. Gating strategy to determine GFP+ single cells in A375 control cells and A375 cells transfected with a GFP plasmid using Fectovir (top panel). Quantification of the percentage of GFP+ cells in control and transfected A375 cells is shown on the bottom. N=2 independent experiments.

Second, to obtain a stable cell line, transfected cells need to be selected to ensure the continuous expression of the sequence of interest. In this case the LentisamV2 backbone harbours a specific cassette for the expression of the puromycin resistance gene, which allows the selection of transfected cells by exposing them to the puromycin antibiotic.

For selection to be efficient cells need to be exposed to a concentration of puromycin that is neither too low, allowing non-transfected cells to survive, nor too high, killing all cells, including those that have been successfully transfected. To find this ideal concentration A375 WT cells were exposed to several concentrations of puromycin – 1 µg/mL, 0.8 µg/mL, 0.6 µg/mL, 0.4 µg/mL and 0.2 µg/mL (**Figure 3.5**). This experiment showed that 1 µg/mL was far too high, with all cells dying 24h after the start of exposure. The same was observed for 0.8 and 0.6 µg/mL. With 0.4 µg/mL all cells were dead at 72h of exposure, ideal for the selection process, while 0.2 µg/mL was too little, with cells only starting to show signs of death after 96h of exposure.

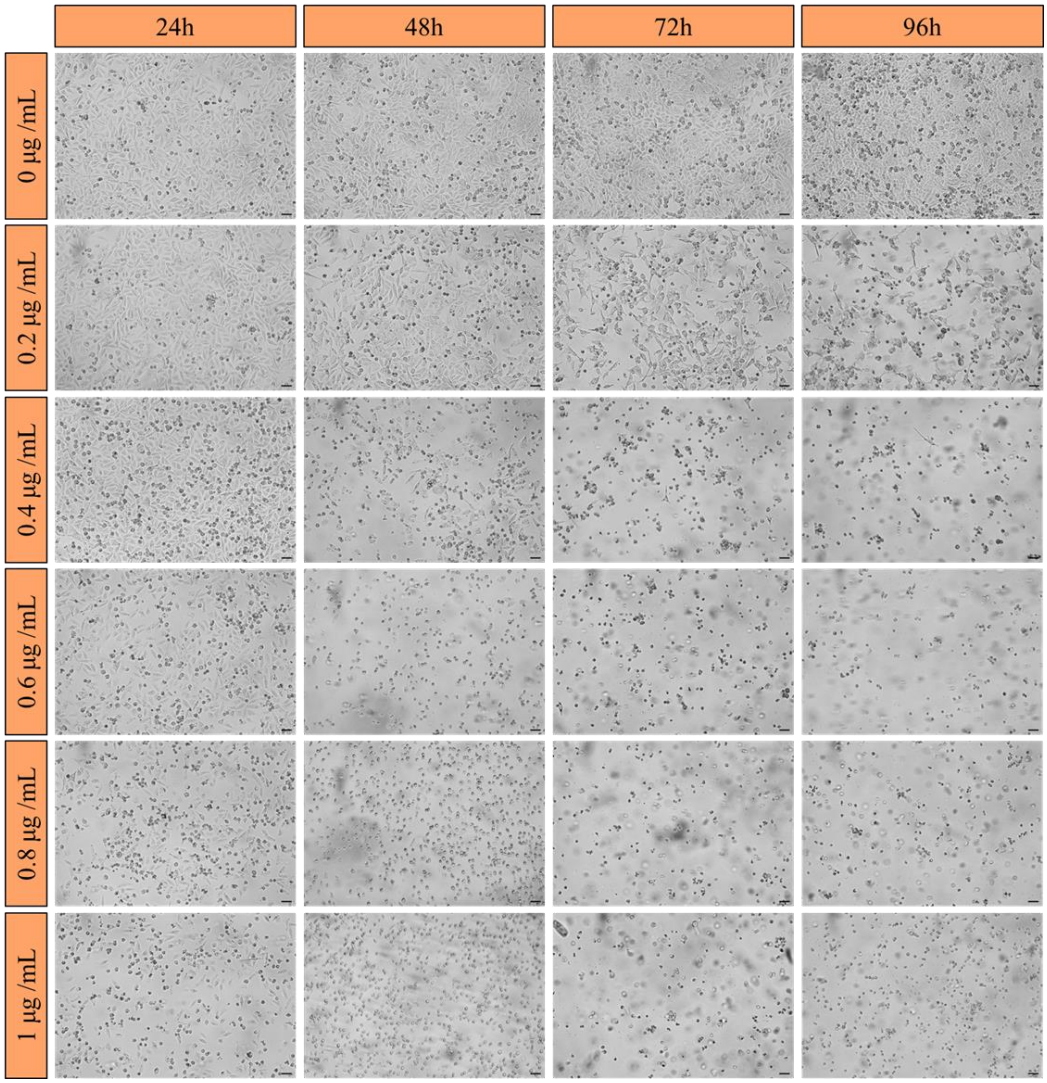

Figure 3.5 – Puromycin selection optimization of A375 melanoma cells. Effectiveness of different concentrations of puromycin on A375 melanoma cells. A375 melanoma cells were maintained in DMEM complete medium with different concentrations of puromycin and monitored for 96h using a brightfield microscope (Olympus CK2). Scalebar = 50 µm.

Since transfection efficiency was acceptable in A375 cells this technique was used to establish stable A375 cells overexpressing *LAMA2*. To do so A375 cells were individually transfected, using Fectovir, with the 3 constructs, each containing a gRNA targeting the *LAMA2* promoter (CRISPRa1, CRISPRa2 or CRISPRa3) or CRISPR scramble plasmids. A GFP plasmid was also co-transfected to help monitor the success of transfection. After successful transfection cells were selected in media with 0.4 µg/mL Puromycin for 96h. Selected cells were then collected, their RNA extracted and used to generate cDNA to check *LAMA2* overexpression via qPCR (**Figure 3.6**). *LAMA2* mRNA expression was significantly increased in cells transfected with the CRISPRa2 plasmid, relative to WT and CRISPRa3 cells ($p < 0.05$). Expression of *LAMA2* was also increased in cells transfected with CRISPRa2 when compared to cells transfected with scramble cells, even though it was not significant ($p = 0.0694$). There were no significant differences in *LAMA2* expression between WT and scrambled cells, suggesting that the control vector has a minimal impact (**Figure 3.6**).

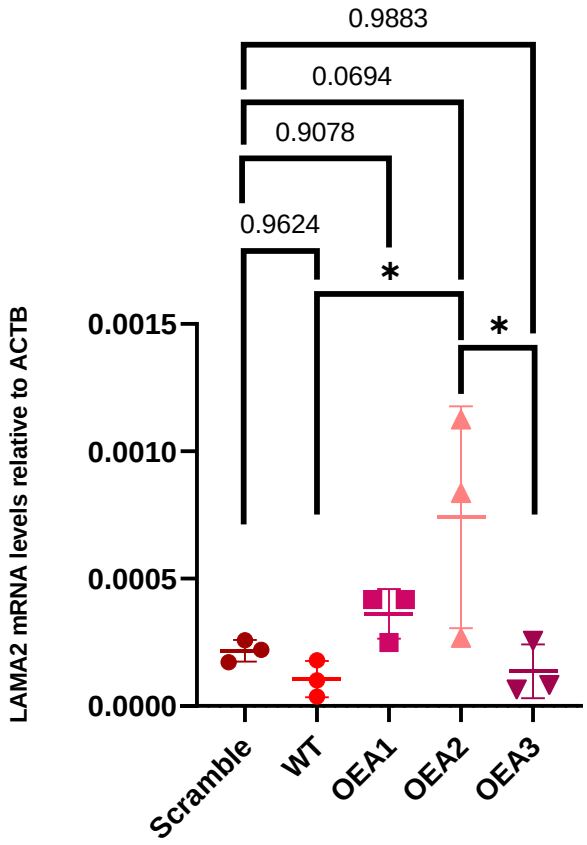

Figure 3.6 – qPCR analysis of *LAMA2* expression levels in A375 WT, Scramble and *LAMA2*-OE cells. The expression of *LAMA2* was analysed in A375 WT and newly established Scramble and LAMA2-OE cells, generated through the transfection with CRISPRa1 (OEA1), CRISPRa2 (OEA2) and CRISPRa3 (OEA3). Graph shows the mRNA levels of *LAMA2* normalized using *ACTB* (encoding actin) as a housekeeping gene. N=3 independent experiments. Statistical analysis was performed using a Two-Way ANOVA with Tukey's multiple comparisons. * = $p<0.05$.

3.3. Establishing 3D spheroid models to dissect the role of *LAMA2* in melanoma

Because the function of the ECM and its components hinges on mechanical properties, the use of models that best mimic them is paramount in the study of ECM components and their role in certain diseases. One of the fundamental aspects behind these properties, not found in traditional monolayer cell culture, is the 3D shape and arrangement of cells and their ECM. Therefore, using 3D models, such as spheroids, may provide a more accurate understanding of the role of the ECM and its components (such as laminin-α2) in tissues and diseases, like melanoma.

To find the best strategy to generate A375 spheroids, two methodologies were employed: the hanging drops and agarose-coated wells. Spheroids from agarose-coated wells were found to be very round and quite cohesive, with their appearance getting better over successive assays. On the other hand, while it was possible to generate spheroids using the hanging drop technique, these were often damaged or destroyed as they were transferred from the drops into agarose-coated wells, making it difficult to assess their morphology or use them in further experiments (**Figure 3.7**). Therefore, the agarose-coated wells method was chosen to generate spheroids in the following experiments.

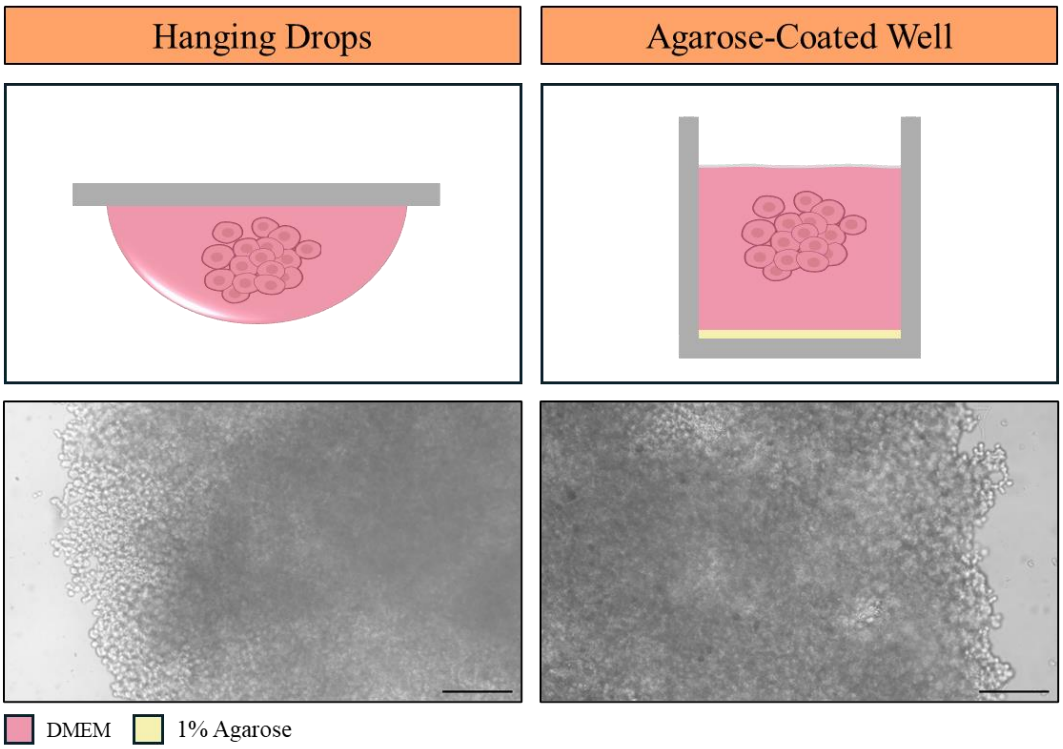

Figure 3.7 – Representative images of A375 WT spheroids generated using the hanging drops and agarose-coated well methods and schematic representation of each method. A375 spheroids were generated using WT cells. Hanging drops spheroids were generated by placing 20 µL drops containing 10000 cells on a Petri dish lid and inverting it over the bottom of the dish. Gravity gathers cells at the bottom of the drop and the liquid-air interface prevents adherence, promoting the formation of spheroids. After 3 days hanging drops, spheroids were transferred to agarose-coated wells. To generate agarose-coated well spheroids the wells of a 96-well plate were covered in 1% agarose in 1xPBS, to prevent cell adherence. Then 80 µL of DMEM were added to each well before a 20 µL drop of a $5x10^5$ cell/mL cell suspension (10000 cells per drop) were also added. In both methods, to further potentiate aggregation, either the 96-well plate or the Petri dish were rotated in an orbital shaker for 10 minutes. Spheroids were left to incubate for 3 days. Spheroids were followed daily by analysis under brightfield microscope (Optika IM-3LD4). Representative images of 3-day old spheroids are shown. Amplification= 10x. Scalebar = 150 µm.

3.4. Analysis of WT and *LAMA2*-KO melanoma spheroids

After establishing the best methodology to generate melanoma spheroids, the role of *LAMA2* in spheroid growth was explored using three *LAMA2*-KO cell lines (KOα, KOθ and KO F), previously established in the laboratory [71]. These cell lines were derived from single-cell clones and were used to validate the phenotypes obtained as being solely due to *LAMA2* mutations and not possible clonal effects.

To determine spheroid growth and proliferation two approaches were used: measurement of spheroid area and the resazurin assay, respectively. To measure area, images of the spheroids were taken on days 3,4, 5 and 6 post seeding (**Figure 3.8A**). These images were then segmented, and the area automatically measured in ImageJ, using a custom script, as described in the Materials and Methods section. Area was then normalized to the average area of the corresponding cell line on the first timepoint, in order to calculate the relative change in size when compared the first measurement, essentially their growth. This was done because different spheroids had to be measured in each timepoint, since the resazurin assays took place at the same time.

For the resazurin assay, the same spheroids were monitored on days 3,4, 5 and 6 post seeding as well. This assay allows the measurement of proliferation over multiple days, by measuring the fluorescence of resorufin, a compound converted from resazurin by metabolically active (and thus viable) cells. The proliferation rate is obtained by dividing the fluorescence counts obtained on each timepoint by the average fluorescence counts of the corresponding cell line in the first timepoint.

In terms of growth no significant differences were found between spheroids generated using different cell lines, although KO cell lines did seem to have slightly, but not significant higher growth than the WT cells. Additionally, growth remained constant at around 1 over the course of the experiment for most cell lines, lines, meaning there were no significant changes in spheroid size over the observed timepoints (**Figure 3.8B**).

Similarly to growth there were no significant differences in proliferation between spheroids of different cell lines. Proliferation also remained constant over the course of the experimental time frame (**Figure 3.8C**).

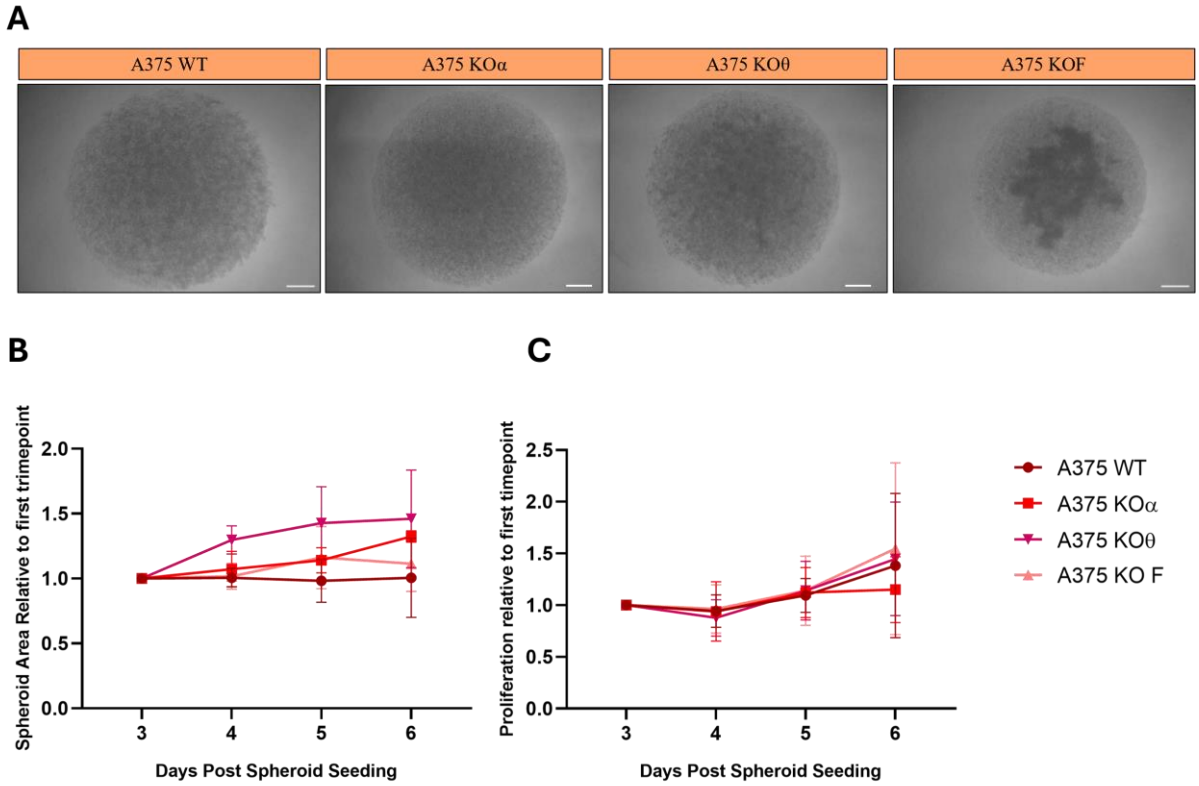

Figure 3.8 – *LAMA2* deletion did not affect spheroid growth or cell proliferation in spheroids. (A) A375 spheroids were generated using WT and *LAMA2*-KO cells. Three independent single cell clones-derived cell lines are represented (A375 KOα, A375 KOθ and A375 KOF). To generate them the wells of a 96-well plate were coated in 1% agarose in PBS, to prevent cell adherence. Then 80 µL of DMEM were added to each well before a 20 µL drop of a $5x10^5$ cell/mL cell suspension (10000 cells per drop) were also added. To further potentiate aggregation the plate was rotated in an orbital shaker for 10 minutes. Spheroids were left to incubate for 3 days. Spheroids were followed daily by analysis under brightfield microscope (Olympus CK2). Representative images of 5-day old spheroids are shown. Amplification = 4x. Scalebar = 250 µm. **(B)** The growth of spheroids established as in A) was monitored on days 3, 4, 5 and 6 post seeding. A custom ImageJ script was used to automatically measure spheroid area using the brightfield images acquired on each day. Area was normalized to the average area on the first timepoint. For each timepoint 4 spheroids were measured. N=4 independent experiments, except for KOα where N=3. Statistical analysis was performed using a Two-way ANOVA with Tukey's multiple comparison test. **(C)** Spheroids were established as in A). Cell proliferation in A375 WT and *LAMA2*-KO spheroids was determined via resazurin assay. The assay was performed on days 3, 4, 5 and 6 post seeding. To determine the proliferation rate fluorescence levels were normalized to the average fluorescence levels of the corresponding cell line in the first timepoint. This was done because the same spheroid could not be used for all timepoints. For each timepoint 4 spheroids were measured. N=4 independent experiments, except for KOα where N=3. Statistical analysis was performed using a Two-way ANOVA with Tukey's multiple comparison test.

Cell death in WT and KO spheroids was analysed by incubating spheroids in 0.5 µg/mL of propidium iodide (PI) in DMEM for 15 minutes. This compound fluoresces (553-723 nm, 618 nm peak) when excited by the correct wavelengths (419-647 nm, 518 nm peak). It is also only permeable to dead cells so only these will be fluorescent under those conditions. PI-stained spheroids were then dissociated exclusively via mechanical action through pipetting and ran through a flow cytometer to obtain the percentage of dead cells (**Figure 3.9A**). Cell death was very low, with no more than 2% of single cells being PI positive (PI+) for any cell line. There were also no differences in cell death between spheroids generated, regardless of the *LAMA2* status (**Figure 3.9B**).

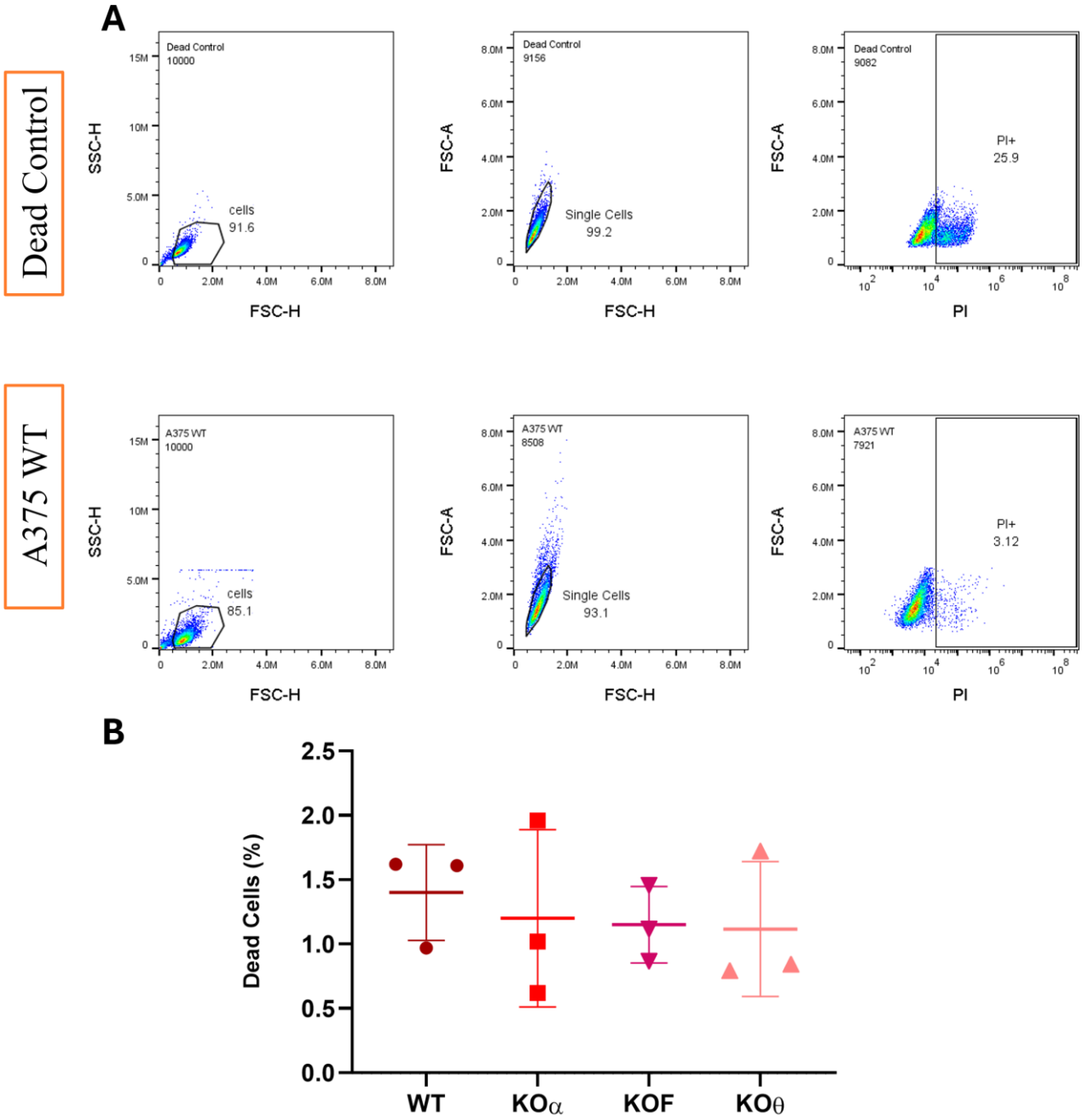

Figure 3.9 – Absence of *LAMA2* did not impact cell death in A375 spheroids. A375 spheroids were stained with propidium iodide to understand if the absence of *LAMA2* impacted cell death in A375 spheroids. Three independent single cell clones-derived cell lines are represented A375 KOα, A375 KOθ and A375 KOF. Propidium iodide is only permeable to dead cells and fluoresces in the 553-723 nm wavelength range when excited by wavelengths in the 419-647 nm range. Flow cytometry can be used to detect and count these fluorescent cells, giving the percentage of dead cells. **(A)** Gating strategy to select PI+ cells. A positive control spheroid that was exposed to 95ºC for 15 minutes, killing a large percentage of cells (top) and an unstained spheroid (bottom) were used to define the gates. **(B)** Percentage of dead cells in spheroids generated using A375 WT and *LAMA2*-KO cells, N=3. Statistical analysis was performed using a One-way ANOVA with Tukey's multiple comparisons.

3.5. Analysis of scramble and *LAMA2*-OE melanoma spheroids

The generation of spheroids using the newly established A375 *LAMA2-OE* and scramble lines was also tested. Considering the higher expression of *LAMA2* in cells transfected with CRISPRa1 (OEA1) and CRISPRa2 (OEA2), the following experiments were performed using only these cell lines. It was possible to successfully establish spheroids using the A375 OEA1, OEA2 and scramble cell lines with the agarose-coated well method (**Figure 3.10A**).

Images of these spheroids were acquired at 3, 4 and 5 days post seeding. The same ImageJ custom script as before was used in these images to segment and measure spheroid area. Growth was then also determined as the area of each spheroid divided by the average area of the corresponding cell line spheroids in the first timepoint. No significant differences in growth between OEA1, OEA2 and scramble spheroids were found, although growth in scramble spheroids did appear to be consistently higher (**Figure 3.10B**).

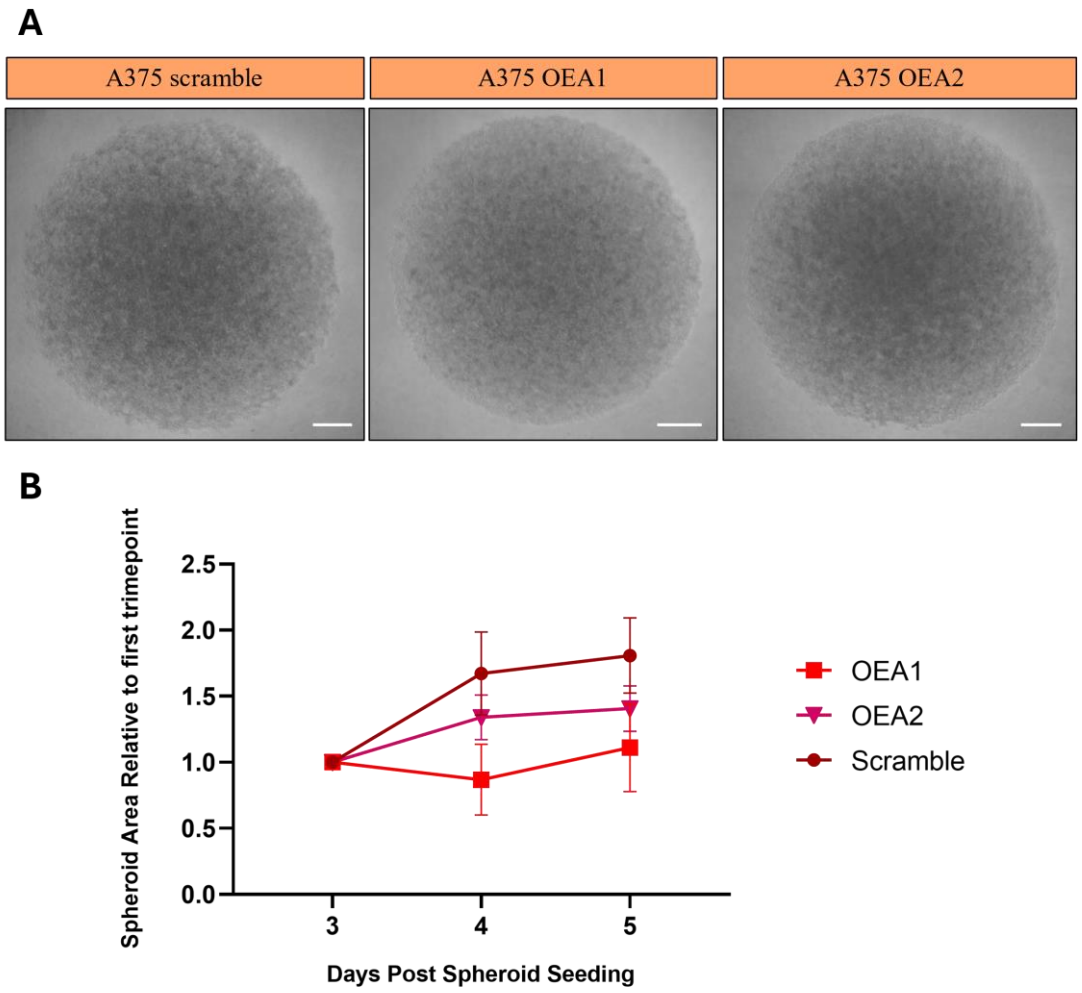

Figure 3.10 – *LAMA2* overexpression did not affect spheroid growth in spheroids. (A) A375 spheroids were generated using scramble and *LAMA2*-OE cells (OEA1 and OEA2). To generate them the wells of a 96-well plate were coated in 1% agarose in 1xPBS, to prevent cell adherence. Then 80 µL of DMEM were added to each well before a 20 µL drop of a $5x10^5$ cell/mL cell suspension (10000 cells per drop) were also added. To further potentiate aggregation the plate was rotated in an orbital shaker for 10 minutes. Spheroids were left to incubate for 3 days before being checked. Spheroids were followed daily by analysis under brightfield microscope (Olympus CK2). Representative images of 5-day old spheroids are shown. Amplification = 4x. Scalebar = 250 µm. **(B)** The growth of spheroids established as in A) was monitored on days 3, 4 and 5 post seeding. A custom ImageJ script was used to automatically measure spheroid area using the brightfield images acquired on each day. Area was normalized to the average area on the first timepoint. For each timepoint 4 spheroids were measured. N=3 independent experiments. Statistical analysis was performed using a Two-way ANOVA with Tukey's multiple comparison test.

Cell death in these spheroids was also quantified using PI as a marker by flow cytometry. In the *LAMA2*-OE cell lines, the use of a GFP plasmid to monitor transfection proved problematic as over time, despite the lack of puromycin resistance in this plasmid, it was able to integrate in the genome and a proportion of cells expressed GFP constitutively. The high intensity of the GFP signal ended up bleeding onto the range of the detector used to detect PI+ (dead) cells. To overcome this WT cells transfected with only GFP were used to create a gate allowing for the analysis of PI+ signal only in GFP negative cells (**Figure 3.11A).** Cell death was found to be very low, with PI+ cells not reaching 2%. There were no significant differences in cell death between scramble, OEA1 and OEA2 spheroids (**Figure 3.11B**).

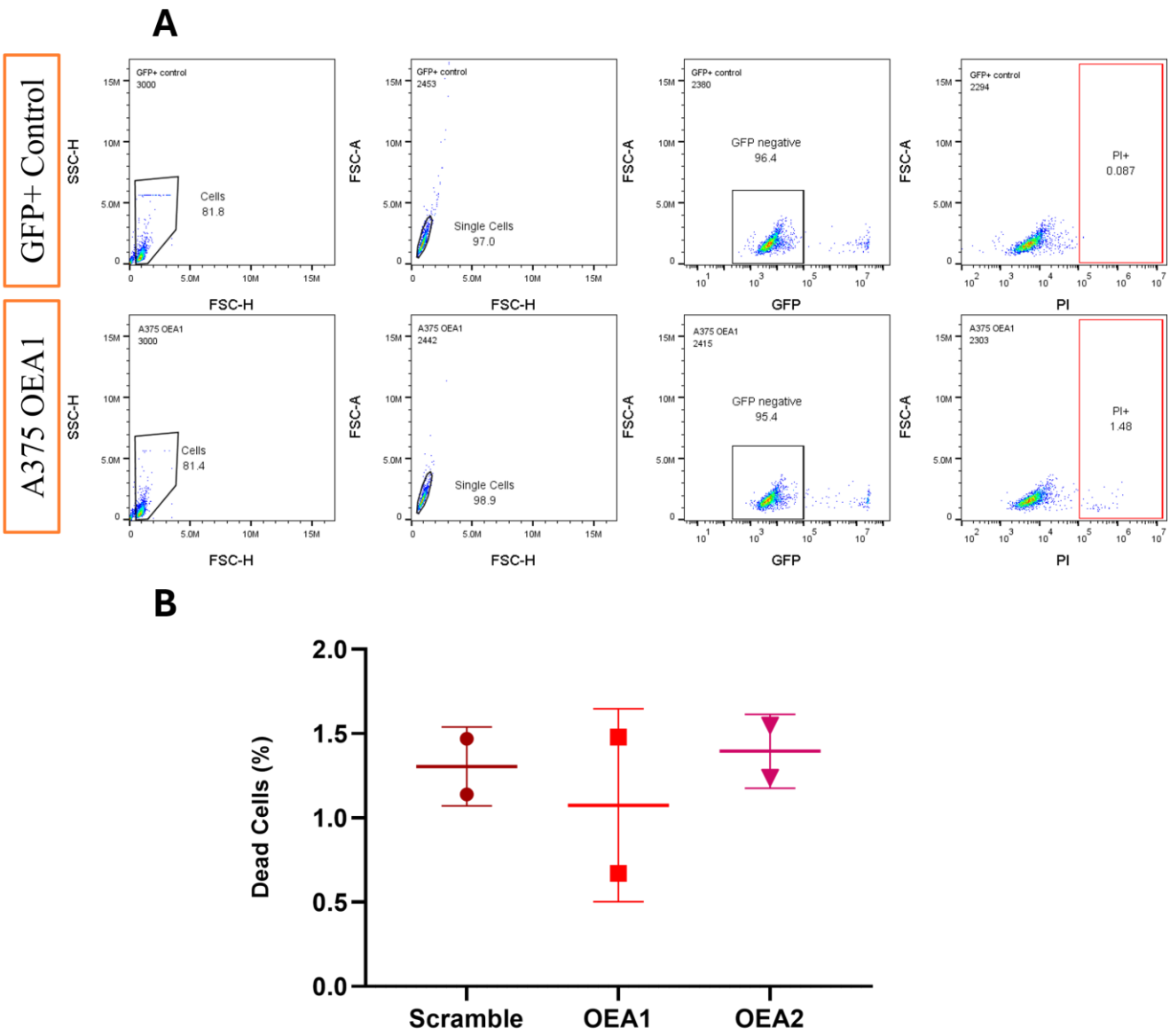

Figure 3.11 – *LAMA2* overexpression did not impact cell death in A375 spheroids. A375 OEA1, OEA2 and scramble spheroids were stained with PI to understand if the overexpression of *LAMA2* impacted cell death. Propidium iodide is only permeable to dead cells and emits fluorescence in the 553-723 nm wavelength range when excited by wavelengths in the 419-647 nm range. Flow cytometry can be used to detect and count these fluorescent cells, giving the percentage of dead cells. **(A)** Gating strategy to select PI+ cells, while excluding GFP+ cells, in a control non stained spheroid (top) and a spheroid generated using A375 WT cells stained with PI. **(B)** Percentage of dead cells treated as in A). N=2 independent experiments. Statistical analysis was performed using a One-way ANOVA with Tukey's multiple comparisons.

3.6. Analysing the impact of *LAMA2* deficiency in ECM-cell signalling

Despite no significant differences being found in *LAMA2*-KO cells in terms of growth and survival in the 3D spheroid model, other aspects were analysed namely the impact of *LAMA2* deficiency in ECM-cell signalling in spheroids.

Spheroids generated using A375 WT and *LAMA2*-KO cells were stained for fibronectin, an important protein for ECM-cell signalling, laminin α2 chain and pan-laminins and observed on a Leica SP5 confocal microscope. As expected *LAMA2*-KO spheroids appear to have less laminin α2 chain signal (**Figures 3.12** and **3.13**). Fibronectin appears to be more present in KOF and WT spheroids with KOα spheroids exhibiting lower levels of this protein, which seems to correlate with the intensity of laminin α2 chain signal. There appeared to be no differences in Pan-laminin levels among the observed WT and KO spheroids (**Figure 3.13A**).

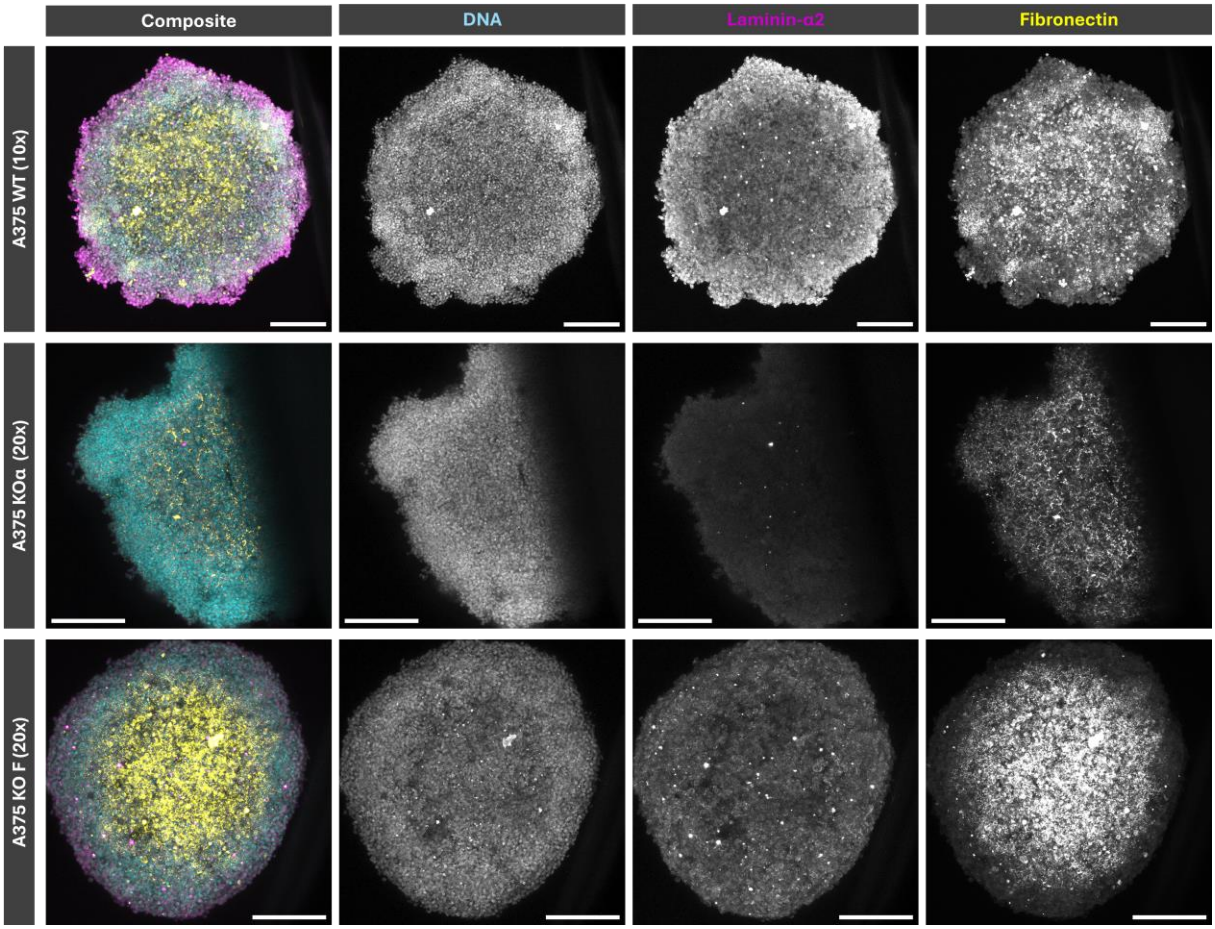

Figure 3.12 – Maximum intensity projection images of immunostained A375 WT and *LAMA2*-KO spheroids (laminin-α2 and fibronectin). Representative images of WT and *LAMA2*-KO spheroids stained with anti-laminin-α2 chain (magenta), anti-fibronectin (yellow) and methyl-green (nuclear staining, cyan). Two independent single cell clones-derived cell lines are represented A375 KOα and A375 KOF. Scale bar = 200 μm.

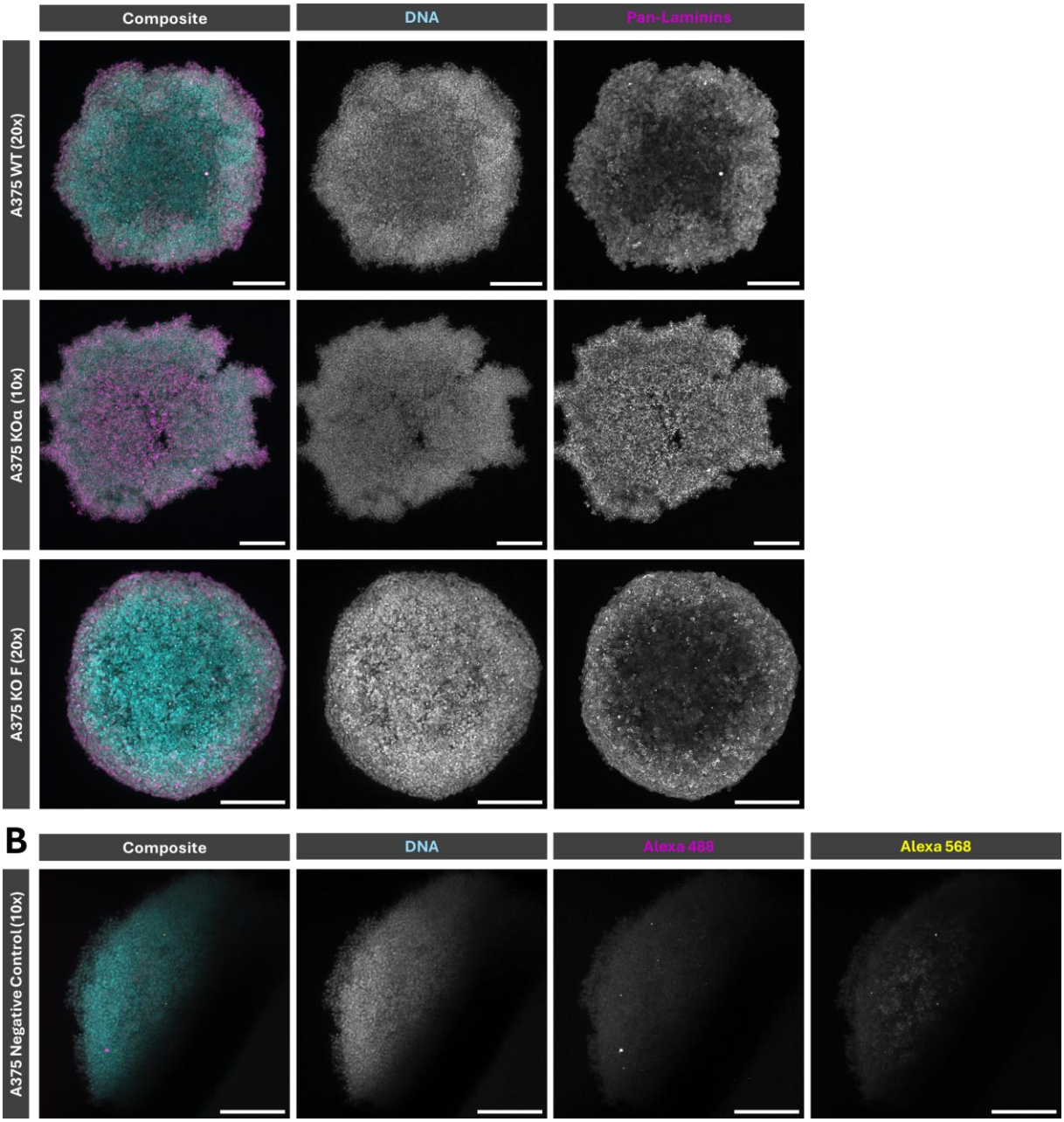

Figure 3.13 – Maximum intensity projection images of immunostained A375 WT and *LAMA2*-KO spheroids (pan-laminins and negative control). (A) Representative images of WT and *LAMA2*-KO spheroids stained with anti-Pan Laminins (magenta) and methyl-green (nuclear staining, cyan). **(B)** Negative control spheroids stained only with methyl green (cyan) and secondary antibodies. Two independent single cell clones-derived cell lines are represented A375 KOα and A375 KOF. Scale bar = 200 μm.

To further understands the impact of *LAMA2* absence in ECM signalling, the activation of the STAT3 pathway was analysed, considering its role in transducing extracellular signals to the nucleus [87], by detecting the levels of phosphorylated STAT3 (P-STAT3) in A375 WT and *LAMA2*-KO cells and spheroids. No significant differences in STAT3 or P-STAT3 protein levels were found between cell lines in either culture method nor were there significant differences between the 2D and 3D cultures (**Figure 3.14**). These results suggest that *LAMA2* deficiency has no impact on the STAT3 pathway.

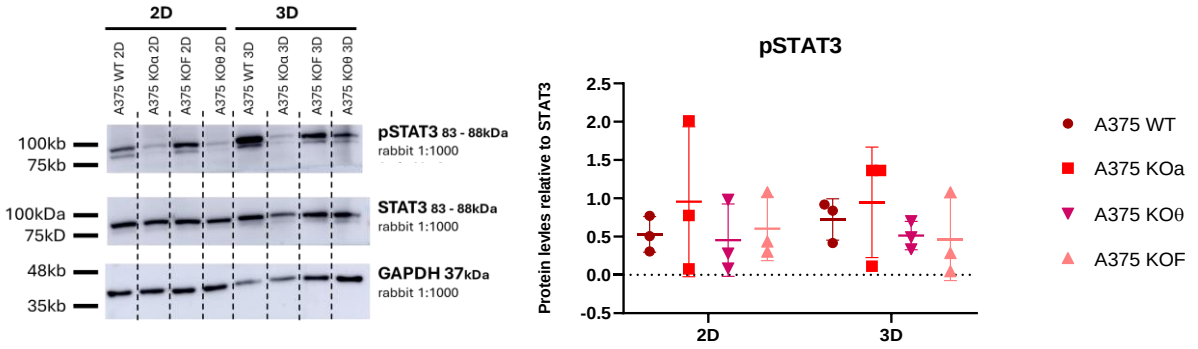

Figure 3.14 – *LAMA2* deficiency did not impact the activation of the STAT3 pathway in A375 cells or spheroids. Analysis of STAT3 phosphorylation on tyrosine 705 (P-STAT3) in cells and spheroids generated using A375 WT and three independent *LAMA2*-KO single cell-clone derived cell lines (KOα, KOθ and KOF). GADPH was used as a loading control. N=3 independent experiments. Statistical analysis was performed using a Two-way ANOVA with Sidak's multiple comparisons test.

Since *MXRA5*, which encodes an ECM protein, was at the top of the altered ECM genes in melanoma when *LAMA2* is altered (**Table 3.1**), its expression was investigated in the A375 WT and KOα, KOθ and KOF spheroids as well as monolayer cells via qPCR. No significant differences were found in *MXRA5* expression levels between WT and *LAMA2*-KO spheroids or cells, nor were there any significant differences between spheroids and monolayer cells, even though there is a tendency for the levels to be decreased in the absence of *LAMA2* (**Figure 3.15A**). However, detection of *MXRA5* expression proved quite difficult, so these results should be taken tentatively.

In addition to *MXRA5*, the expression of *MAPK6* was also investigated via qPCR in A375 WT and KO spheroids and monolayer cells. This gene encodes a kinase that is well-known to play a role in the transduction of extracellular signals to the nucleus. Moreover, the MAPK pathway appears to be regulated by MXRA5, and LAMA2 has been shown to regulate the progression of breast cancer through this pathway as well [56,88]. Like *MXRA5* no significant differences in the expression of *MAPK6* were found between WT and *LAMA2*-KO cells or spheroids nor between monolayer cells and spheroids (**Figure 3.15B**).

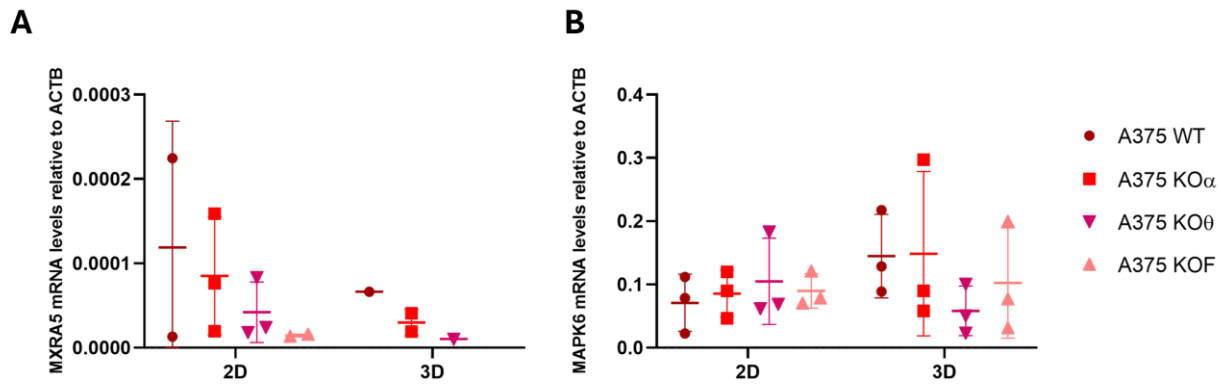

Figure 3.15 – qPCR analysis of expression levels of *MXRA5* and *MAPK6* in A375 WT and *LAMA2*-KO cells and spheroids. The expression of *MXRA5* and *MAPK6* was analysed in A375 WT and *LAMA2* KO cells (2D) and spheroids (3D) via qPCR. Three independent single cell clones-derived cell lines are represented A375 KOα, A375 KOθ and A375 KOF. **(A)** Expression levels of *MXRA5*, normalized using *ACTB* as a housekeeping gene. N=1-3 independent experiments. In A375 KOF spheroids *MXRA5* failed to amplify. **(B)** Expression levels of *MAPK6*, normalized using *ACTB* as a housekeeping gene. N=3 independent experiments. Statistical analysis was performed using a Two-Way ANOVA with Tukey's multiple comparisons.

3.7. Analysing the impact of *LAMA2* overexpression in ECM-cell signalling

Expression levels of *MXRA5* and *MAPK6* were also investigated in *LAMA2*-OE (OEA1 and OEA2) and scramble monolayer cells and spheroids. No significant differences in expression were found on either gene between cell lines or between culture methods (**Figure 3.16**). Nevertheless, expression of *MXRA5* gene showed a tendency to be increased in *LAMA2*-OE cells (**Figure 3.16A**). Like before, however, *MXRA5* was quite difficult to detect so results should be taken in a tentative manner.

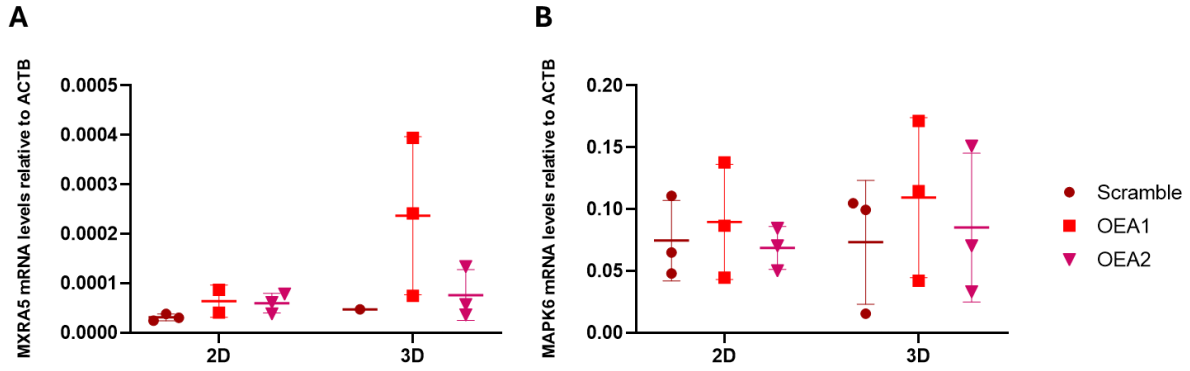

Figure 3.16 – qPCR analysis of expression levels of *MXRA5* and *MAPK6* in A375 Scramble and *LAMA2*-OE cells and spheroids. The expression of *MXRA5* and *MAPK6* was analysed in A375 Scramble and *LAMA2*-OE cells (2D) and spheroids (3D) via qPCR. **(A)** Expression levels of *MXRA5*, normalized using *ACTB* as a housekeeping gene. N=1-3 independent experiments. **(B)** Expression levels of *MAPK6*, normalized using *ACTB* as a housekeeping gene. N=3 independent experiments. Statistical analysis was performed using a Two-Way ANOVA with Tukey's multiple comparisons.

4. Discussion

The ECM plays a very important role in cancer. It can regulate many of the hallmarks of this disease, such as sustained proliferation, apoptosis resistance and immune evasion [36]. *LAMA2* has also been shown to play a role in many cancers. This includes melanoma, where *LAMA2* was found to be altered in 25% of samples in a cBioPortal analysis (**Figure 3.1B**). Still, the roles of the ECM and *LAMA2* in tumour progression remain somewhat unexplored.

To dissect this role the use of appropriate models is necessary. While classic monolayer cell cultures have been useful in furthering the understanding of many biological processes in mechanisms and disease, they are also not always the most accurate [57–59,63,64]. This is especially true when attempting to study the role of ECMs, whose function is regulated not only by their biochemical properties but also mechanical ones. Specifically, *in vivo* ECMs organize in a 3D manner, which tend to allow for more and more complex cell-cell and cell-matrix interactions. Therefore, one good option when studying the role of ECM and its components, such as laminins, is the use of *in vitro* 3D models [57–59,63,64].

One example of a 3D model are cellular spheroids or simply spheroids. These are self-assembled cell aggregates that usually take on a spherical shape. There are many strategies and techniques available to generate spheroids, varying in ease-of-use, cost and efficiency. This makes spheroids an attractive 3D model, since they may be generated in both an efficient and cost-effective manner [63,64,89].

This project sought to establish such 3D models to study the role of ECM in tumour progression, specifically in melanoma (**Figure 3.7**). The generation of spheroids was tested on A375 human melanoma cell lines, both WT and *LAMA2*-KO. Two methods were tested: the hanging drops method, in which cells are suspended in drops and gravity promotes their aggregation in spheroids; and the agarose-covered well method, in which cells are plated in wells of a 96-well plate covered in 1% agarose in 1xPBS, which prevents cells from adhering to the bottom and thus promotes the formation of spheroids. While both methods led to the successful generation of spheroids, those generated using the hanging drops method appeared to be less cohesive and more fragile (**Figures 3.7** and **3.8**). Additionally, after the initial formation period, they had to be transferred to agarose covered wells. This transference step often led to the destruction of spheroids. In contrast, no extra handling was necessary with the agarose-coated well spheroids. This fact made this method preferable to the hanging drops and it was used throughout the remainder of the project. It also highlighted that, even though A375 can form spheroids, these are somewhat loose structures, which should be considered depending on the type of experiment. A possible way to improve this could be the use of ultra-low attachment spheroid specific plates or co-culture with appropriate cell lines, which could help stabilize these structures.

After establishing the best spheroid generation method, A375 WT and *LAMA2*-KO spheroids were used in several experiments to evaluate various characteristics related to tumour progression. Namely proliferation was evaluated using the resazurin assay, cell death was determined using PI staining and flow cytometry and growth of spheroids was determined by measuring their area.

Contrary to previous results of the host laboratory using 2D culture, the absence of *LAMA2* did not affect proliferation in A375 spheroids (**Figure 3.8C**). Additionally, proliferation levels were stable during the experimental timeframe with only a slight but non-significant increase overtime, regardless of the genotype (**Figure 3.8C**). Similar results were observed for growth, although interestingly WT spheroids generally presented lower changes in area compared to *LAMA2*-KO spheroids (**Figure 3.8B**). These results contrast with the observation using 2D cultures, where *LAMA2*-KO cells showed lower proliferation rate, when compared to WT counterparts [90]. In addition, *LAMA2* deletion in mouse C2C12 myoblast cell line also led to a significant reduction in proliferation [91]. Differences between 2D and 3D, could be explained, for example, by the different dynamics of cell growth. It is possible that in 3D culture later time points need to be analysed. It is important to note that there was a large amount of variability in both growth and proliferation between experiments, as can be seen by the wide error bars

(**Figures 3.8B** and **3.8C**). This was not the case for spheroids of the same line generated for the same assay. What leads to this high inter-experiment variability is unclear. One possibility is that it is caused by slight variations in the conditions of each experiment. Another potential explanation is that this variability is due to the cells themselves, which change over time. A well-known problem in cell culture is genetic drift. Over time, as cell populations are maintained in culture, with successive cycles of expansion and bottlenecking, they may acquire various mutations that can change how cells behave [92–94]. With their inherent genetic instability this is likely amplified in tumour cell lines, like the A375 melanoma line. In fact, this is a common observation in tumours, which are known to be composed of highly heterogeneous cell populations [95–97]. To counter this, cells should be defrosted and left in culture for the same amount of time. In addition to proliferation and growth, there were also no differences in cell death between A375 WT and *LAMA2*-KO spheroids, with cell death being remarkably low in all of them, never going past 2% (**Figure 3.9B**). This indicates that the 3D structure does not impact negatively on cell viability and that nutrients and oxygen are able to be delivered to all cells. In accordance, analysis of images of PI-stained spheroids did not reveal the presence of a necrotic core (**Figure S3**), unlike what is expected in spheroids [89]. This has been further confirmed by Ki-67 staining, which shows proliferating cells, of spheroid paraffin sections (*unpublished data*).

The impact of *LAMA2* in other ECM components in A375 spheroids was also evaluated. As expected, KO spheroids had less laminin-α2 chain signal than WT spheroids, with KOF spheroids appearing to have slightly more than KOα spheroids (**Figure 3.12**). This seemed to correlate with fibronectin signal, which appeared to be more intense in WT and KOF spheroids (**Figure 3.12**). The role of fibronectin in tumour progression, according to the literature, does not appear to be linear. Some work suggests it has a protective effect while others appear to show fibronectin contributes to tumour progression by inhibiting cell death and promoting invasion and proliferation [98–100]. As such what its relationship with *LAMA2* means in this context is difficult to assess. More work needs to be done to both confirm this association and understand what it may mean for other characteristics associated with tumour progression, such as migration and cell proliferation. There appeared to be no differences in Pan-Laminin signal (**Figure 3.13A**), which could indicate that in the absence of *LAMA2* other laminins are elevated, to compensate for its loss. This has been observed to occur in the absence of *LAMA2* and other laminins in other diseases [47,101–104].

An important part of how the ECM impacts tumour progression is cell-matrix communication. To evaluate how the absence of *LAMA2* affects this communication the activation of STAT3 via Y705 phosphorylation was analysed. STAT3 is not only responsible for the transduction of extracellular signals into transcriptional changes, but also encoded by a well-known oncogene, with its constitutive activation known to aid in the transformation of normal cells into tumour cells [38,41–43]. It has also been shown to be overactivated in melanoma, where it promotes cell survival and proliferation [105]. No significant differences in P-STAT3 levels were found in A375 WT and *LAMA2*-KO cells and spheroids, either between cell lines or culture methods (**Figure 3.14**). Previous results in the laboratory had shown an increase of STAT3 activation in *LAMA2*-CMD models [106], but other previous work in A375 cells also found no significant increase in STAT3 activation using only 2D model of A375 [90].

Besides the establishment of 3D models using the already established A375 WT and *LAMA2*-KO cell lines, this project also had the objective of establishing a new A375 *LAMA2*-OE cell line. The establishment of this line is an important step in furthering the understanding of the effect of laminin-α2 in tumour progression, by allowing to explore how its excess affects tumorigenesis. One of the generated plasmids (OEA2) proved to be successful, with cells transfected with this plasmid having significantly higher *LAMA2* expression than WT cells and a clear tendency for higher expression than cells transfected with the scramble gRNA (**Figure 3.6**). These results are important to show that this methodology is efficient in modulating *LAMA2* promoter activity and are critical for following up studies.

Similar to the results obtained with *LAMA2*-KO cell lines, there were no significant differences in growth between OE and scramble spheroids. However, it is interesting to note that scramble spheroids consistently showed higher growth, relative to OE cells (**Figure 3.10**). Taken together with the previous observation that *LAMA2*-KO spheroids presented higher growth than WT, this may hint that *LAMA2* has a negative impact on the growth of tumour cells, which could become more apparent over a longer timeframe, although this relation needs to be verified through further experiments. In fact, laminin-α2 has been shown to have a protective effect in hepatocarcinoma, to be negatively correlated with invasion aggressiveness in pituitary adenoma and to inhibit tumour growth in breast cancer [49,55,56,107]. Furthermore, BMs are a marker of epithelial structures and so, as key BM components, laminins are likely important in promoting a more epithelial-like phenotype [108]. This phenotype is antithetical to the mesenchymal phenotype characteristic of metastatic tumour cells, which have gone through epithelial-to-mesenchymal transition (EMT) and so the promotion of this epithelial phenotype may represent another way laminin-α2 prevents tumour progression [26,109]. There were also no differences in cell death between scramble and *LAMA2*-OE spheroids and once again cell death was remarkably low across the different cell lines (<2%) (**Figure 3.11B**). Taken with the previous results in WT and *LAMA2*-KO cells, it seems *LAMA2* does not affect cell death in A375 melanoma spheroids. This goes against previous results in monolayer A375 cell that show increased cell death in *LAMA2*-KO cell lines [90]. Additionally other studies have shown that higher *LAMA2* levels are expected to increase cell death in cancer cells, which contradicts both sets of results [56]. It is not clear why this is, though an interesting possibility to consider is that the discrepancy between monolayer and spheroid culture results could be due to the 3D versus 2D configuration. Comparative experiments between spheroids and monolayer cells would be needed to test this hypothesis. As mentioned above, the timeframe of the analysis should also be extended to more accurately evaluate the role of *LAMA2* in cell proliferation and death.

In addition to verifying that *LAMA2* is altered in a large portion of melanoma samples, cBioPortal was also used to compare melanoma samples with altered and unaltered *LAMA2*, and identify potential GOIs [76–78]. The number one most significantly altered gene identified was *MXRA5*, a member of the MXRA family of proteins and which is involved in cell adhesion and ECM remodelling [81–83,110]. *MXRA5* has also been implicated in the process of tumorigenesis in colorectal, pancreatic and non-small cell lung cancer [81–83,110]. There are, however, not many studies exploring the role of this gene in cancer and, in fact, none were found exploring it in melanoma. This made it an interesting target to explore using the A375 spheroids. Other than *MXRA5, MAPK6* was also chosen as an interesting target to explore. The MAPK pathway, responsible for the regulation of cell proliferation is already well known to be involved in tumour progression. In fact, it is very commonly altered in melanoma, with the extremely common BRAF mutation found in more than 50% of melanoma cases affecting this pathway [7,13,14]. Additionally, both *LAMA2* and *MXRA5* seems to play their role in cancer by regulating the MAPK/ERK pathway, which made exploring this pathway more interesting [56,81,83,88] . *MAPK6* was specifically chosen because it was flagged as a GOI in melanoma in a previous cBioPortal analysis (*unpublished data*). Analysing the expression of both *MXRA5* and *MAPK6* did not reveal significant differences between WT and *LAMA2*-KO or between scramble and *LAMA2*-OE cell lines, neither in 2D or 3D cultures (**Figures 3.15** and **3.16**). Nevertheless, *MXRA5* showed a very slight tendency to have decreased expression in KO cells and spheroids and increased expression in OE cells and spheroids. An increase in the expression of this gene has been linked to lower patient survival and an increase of cell proliferation and migration in pancreatic cancer [110]. That would mean that a deficiency in *LAMA2* leads to an amelioration of tumour progression in melanoma. This contradicts some of the literature, which shows *LAMA2* to negatively impact cancer cells [49,55,56,107] , but would be consistent with previous results of the host laboratory that show a decrease in proliferation and migration, as well as an increase in cell death in *LAMA2*-KO A375 cells cultured in 2D [90]. However, it is important to note that *MXRA5* proved difficult to detect, with technical replicates often having a large disparity between them or the presence

of this gene outright not being detected in some replicates. As such, these results are not conclusive and should be taken tentatively, with more experiments and optimizations needed to draw solid conclusions.

Overall, the project was successful in establishing *in vitro* 3D models to study the role of ECM and particularly *LAMA2* in tumour progression. Additionally, the obtained preliminary data on spheroid characterisation can serve as a basis for future work and can provide insight into how to improve and optimise the use of this model in future work. The successful generation of a *LAMA2*-OE cell line also represents an important stepping stone for future research in the role of this gene in melanoma, and even in other cancers and diseases.

5. References

1. Bray, F. *et al.* Global cancer statistics 2022: GLOBOCAN estimates of incidence and mortality worldwide for 36 cancers in 185 countries. *CA: A Cancer Journal for Clinicians* **74**, 229–263 (2024).
2. Bray, F., Laversanne, M., Weiderpass, E. & Soerjomataram, I. The ever-increasing importance of cancer as a leading cause of premature death worldwide. *Cancer* **127**, 3029–3030 (2021).
3. Linos, E., Swetter, S. M., Cockburn, M. G., Colditz, G. A. & Clarke, C. A. Increasing Burden of Melanoma in the United States. *J Invest Dermatol* **129**, 1666–1674 (2009).
4. Matthews, N. H., Li, W.-Q., Qureshi, A. A., Weinstock, M. A. & Cho, E. Epidemiology of Melanoma. *Exon Publications* 3–22 (2017) doi:10.15586/codon.cutaneousmelanoma.2017.ch1.
5. Belter, B., Haase-Kohn, C. & Pietzsch, J. Biomarkers in Malignant Melanoma: Recent Trends and Critical Perspective. in *Cutaneous Melanoma: Etiology and Therapy* (eds. Ward, W. H. & Farma, J. M.) (Codon Publications, Brisbane (AU), 2017).
6. Davis, L. E., Shalin, S. C. & Tackett, A. J. Current state of melanoma diagnosis and treatment. *Cancer Biology & Therapy* **20**, 1366–1379 (2019).
7. Schadendorf, D. *et al.* Melanoma. *The Lancet* **392**, 971–984 (2018).
8. Amalinei, C. *et al.* The Interplay between Tumour Microenvironment Components in Malignant Melanoma. *Medicina* **58**, 365 (2022).
9. Spillane, J., Henderson, M. & McArthur, G. A. Melanoma. in *PET/CT in Melanoma* (eds. Hofman, M. S. & Hicks, R. J.) 1–8 (Springer International Publishing, Cham, 2017). doi:10.1007/978-3-319-54741-1_1.
10. Cichorek, M., Wachulska, M., Stasiewicz, A. & Tymińska, A. Skin melanocytes: biology and development. *Postepy Dermatol Alergol* **30**, 30–41 (2013).
11. Dzwierzynski, W. W. Melanoma Risk Factors and Prevention. *Clinics in Plastic Surgery* **48**, 543–550 (2021).
12. Garbe, C. & Leiter, U. Melanoma epidemiology and trends. *Clinics in Dermatology* **27**, 3–9 (2009).
13. Tímár, J. & Ladányi, A. Molecular Pathology of Skin Melanoma: Epidemiology, Differential Diagnostics, Prognosis and Therapy Prediction. *International Journal of Molecular Sciences* **23**, 5384 (2022).
14. Eddy, K., Shah, R. & Chen, S. Decoding Melanoma Development and Progression: Identification of Therapeutic Vulnerabilities. *Front. Oncol.* **10**, (2021).
15. Frisone, D., Friedlaender, A., Malapelle, U., Banna, G. & Addeo, A. A *BRAF* new world. *Critical Reviews in Oncology/Hematology* **152**, 103008 (2020).
16. Randic, T., Kozar, I., Margue, C., Utikal, J. & Kreis, S. NRAS mutant melanoma: Towards better therapies. *Cancer Treatment Reviews* **99**, 102238 (2021).
17. Zhang, W. & Liu, H. T. MAPK signal pathways in the regulation of cell proliferation in mammalian cells. *Cell Res* **12**, 9–18 (2002).
18. Martini, M., De Santis, M. C., Braccini, L., Gulluni, F. & Hirsch, E. PI3K/AKT signaling pathway and cancer: an updated review. *Annals of Medicine* **46**, 372–383 (2014).
19. Hynes, R. O. The Extracellular Matrix: Not Just Pretty Fibrils. *Science* **326**, 1216–1219 (2009).
20. Cox, T. R. The matrix in cancer. *Nat Rev Cancer* **21**, 217–238 (2021).
21. Lu, P., Weaver, V. M. & Werb, Z. The extracellular matrix: A dynamic niche in cancer progression. *Journal of Cell Biology* **196**, 395–406 (2012).
22. Frantz, C., Stewart, K. M. & Weaver, V. M. The extracellular matrix at a glance. *Journal of Cell Science* **123**, 4195–4200 (2010).

23. Walker, C., Mojares, E. & Del Río Hernández, A. Role of Extracellular Matrix in Development and Cancer Progression. *International Journal of Molecular Sciences* **19**, 3028 (2018).
24. Xiong, G.-F. & Xu, R. Function of cancer cell-derived extracellular matrix in tumor progression. *jcmt* **2**, 357–364 (2016).
25. Jayadev, R. & Sherwood, D. R. Basement membranes. *Current Biology* **27**, R207–R211 (2017).
26. Banerjee, S. *et al.* Multiple roles for basement membrane proteins in cancer progression and EMT. *Eur J Cell Biol* **101**, 151220 (2022).
27. Girigoswami, K., Saini, D. & Girigoswami, A. Extracellular Matrix Remodeling and Development of Cancer. *Stem Cell Rev and Rep* **17**, 739–747 (2021).
28. Larsen, M., Artym, V. V., Green, J. A. & Yamada, K. M. The matrix reorganized: extracellular matrix remodeling and integrin signaling. *Current Opinion in Cell Biology* **18**, 463–471 (2006).
29. Rohani, M. G. & Parks, W. C. Matrix remodeling by MMPs during wound repair. *Matrix Biology* **44–46**, 113–121 (2015).
30. Lu, P., Takai, K., Weaver, V. M. & Werb, Z. Extracellular Matrix Degradation and Remodeling in Development and Disease. *Cold Spring Harb Perspect Biol* **3**, a005058 (2011).
31. Sonbol, H. S. Extracellular Matrix Remodeling in Human Disease. *Journal of Microscopy and Ultrastructure* **6**, 123 (2018).
32. Hanahan, D. & Weinberg, R. A. The Hallmarks of Cancer. *Cell* **100**, 57–70 (2000).
33. Hanahan, D. & Weinberg, R. A. Hallmarks of Cancer: The Next Generation. *Cell* **144**, 646–674 (2011).
34. Hanahan, D. Hallmarks of Cancer: New Dimensions. *Cancer Discovery* **12**, 31–46 (2022).
35. Bonnans, C., Chou, J. & Werb, Z. Remodelling the extracellular matrix in development and disease. *Nat Rev Mol Cell Biol* **15**, 786–801 (2014).
36. Pickup, M. W., Mouw, J. K. & Weaver, V. M. The extracellular matrix modulates the hallmarks of cancer. *EMBO reports* **15**, 1243–1253 (2014).
37. Zhou, J., Yi, Q. & Tang, L. The roles of nuclear focal adhesion kinase (FAK) on Cancer: a focused review. *Journal of Experimental & Clinical Cancer Research* **38**, 250 (2019).
38. Bromberg, J. F. *et al.* Stat3 as an Oncogene. *Cell* **98**, 295–303 (1999).
39. Sieg, D. J. *et al.* FAK integrates growth-factor and integrin signals to promote cell migration. *Nat Cell Biol* **2**, 249–256 (2000).
40. Sulzmaier, F. J., Jean, C. & Schlaepfer, D. D. FAK in cancer: mechanistic findings and clinical applications. *Nat Rev Cancer* **14**, 598–610 (2014).
41. Wang, H.-Q. *et al.* STAT3 pathway in cancers: Past, present, and future. *MedComm* **3**, e124 (2022).
42. Ma, J., Qin, L. & Li, X. Role of STAT3 signaling pathway in breast cancer. *Cell Commun Signal* **18**, 33 (2020).
43. Yu, H., Pardoll, D. & Jove, R. STATs in cancer inflammation and immunity: a leading role for STAT3. *Nat Rev Cancer* **9**, 798–809 (2009).
44. Hohenester, E. Structural biology of laminins. *Essays in Biochemistry* **63**, 285–295 (2019).
45. Rousselle, P. & Scoazec, J. Y. Laminin 332 in cancer: When the extracellular matrix turns signals from cell anchorage to cell movement. *Seminars in Cancer Biology* **62**, 149–165 (2020).
46. Pompili, S., Latella, G., Gaudio, E., Sferra, R. & Vetuschi, A. The Charming World of the Extracellular Matrix: A Dynamic and Protective Network of the Intestinal Wall. *Front. Med.* **8**, (2021).
47. Barraza-Flores, P., Bates, C. R., Oliveira-Santos, A. & Burkin, D. J. Laminin and Integrin in LAMA2-Related Congenital Muscular Dystrophy: From Disease to Therapeutics. *Front. Mol. Neurosci.* **13**, (2020).

48. Sakr, H. M. *et al.* Whole-body muscle MRI characteristics of LAMA2-related congenital muscular dystrophy children: An emerging pattern. *Neuromuscular Disorders* **31**, 814–823 (2021).
49. Hu, J. & Li, S. The Role of Lama2 in Cancer: Current Perspectives. *Cancer Res. J.* **10**, 85–88 (2022).
50. Maltseva, D. V. & Rodin, S. A. Laminins in Metastatic Cancer. *Mol Biol* **52**, 350–371 (2018).
51. Liang, X. *et al.* Targeted next-generation sequencing identifies clinically relevant somatic mutations in a large cohort of inflammatory breast cancer. *Breast Cancer Res* **20**, 88 (2018).
52. Vossen, D. M. *et al.* Comparative genomic analysis of oral versus laryngeal and pharyngeal cancer. *Oral Oncol* **81**, 35–44 (2018).
53. Jhunjhunwala, S. *et al.* Diverse modes of genomic alteration in hepatocellular carcinoma. *Genome Biology* **15**, 436 (2014).
54. Yang, P. & Diao, B. Comprehensive Analysis of the Expression and Prognosis for Laminin Genes in Ovarian Cancer. *Pathol. Oncol. Res.* **27**, 1609855 (2021).
55. Wang, R.-Q. *et al.* Expression and methylation status of LAMA2 are associated with the invasiveness of nonfunctioning PitNET. *Ther Adv Endocrinol Metab* **10**, 2042018818821296 (2019).
56. Li, S. *et al.* Epigenetic regulation of LINC01270 in breast cancer progression by mediating LAMA2 promoter methylation and MAPK signaling pathway. *Cell Biol Toxicol* **39**, 1359–1375 (2023).
57. Antoni, D., Burckel, H., Josset, E. & Noel, G. Three-Dimensional Cell Culture: A Breakthrough in Vivo. *International Journal of Molecular Sciences* **16**, 5517–5527 (2015).
58. Białkowska, K., Komorowski, P., Bryszewska, M. & Miłowska, K. Spheroids as a Type of Three-Dimensional Cell Cultures—Examples of Methods of Preparation and the Most Important Application. *International Journal of Molecular Sciences* **21**, 6225 (2020).
59. Kim, J., Koo, B.-K. & Knoblich, J. A. Human organoids: model systems for human biology and medicine. *Nat Rev Mol Cell Biol* **21**, 571–584 (2020).
60. Habanjar, O., Diab-Assaf, M., Caldefie-Chezet, F. & Delort, L. 3D Cell Culture Systems: Tumor Application, Advantages, and Disadvantages. *International Journal of Molecular Sciences* **22**, 12200 (2021).
61. Kramer, N. *et al.* In vitro cell migration and invasion assays. *Mutat Res* **752**, 10–24 (2013).
62. Lv, D., Hu, Z., Lu, L., Lu, H. & Xu, X. Three-dimensional cell culture: A powerful tool in tumor research and drug discovery (Review). *Oncology Letters* **14**, 6999–7010 (2017).
63. Lin, R.-Z. & Chang, H.-Y. Recent advances in three-dimensional multicellular spheroid culture for biomedical research. *Biotechnology Journal* **3**, 1172–1184 (2008).
64. Kyriakopoulou, K., Koutsakis, C., Piperigkou, Z. & Karamanos, N. K. Recreating the extracellular matrix: novel 3D cell culture platforms in cancer research. *The FEBS Journal* **n/a**,.
65. Brüningk, S. C., Rivens, I., Box, C., Oelfke, U. & ter Haar, G. 3D tumour spheroids for the prediction of the effects of radiation and hyperthermia treatments. *Sci Rep* **10**, 1653 (2020).
66. Senrung, A. *et al.* 3D tumor spheroids: morphological alterations a yardstick to anti-cancer drug response. *In vitro models* **2**, 219–248 (2023).
67. Conti, S. *et al.* CAFs and Cancer Cells Co-Migration in 3D Spheroid Invasion Assay. in *The Epithelial-to Mesenchymal Transition: Methods and Protocols* (eds. Campbell, K. & Theveneau, E.) 243–256 (Springer US, New York, NY, 2021). doi:10.1007/978-1-0716-0779-4_19.
68. Tumor Spheroid-Based Migration Assays for Evaluation of Therapeutic Agents | SpringerLink. https://link.springer.com/protocol/10.1007/978-1-62703-311-4_16.
69. Nazari, S. S. Generation of 3D Tumor Spheroids with Encapsulating Basement Membranes for Invasion Studies. *Curr Protoc Cell Biol* **87**, e105 (2020).

70. Hubrecht, R. C. & Carter, E. The 3Rs and Humane Experimental Technique: Implementing Change. *Animals (Basel)* **9**, 754 (2019).
71. Fonseca, I. C. F. O. da. Characterizing the impact of LAMA2-deficiency in cancer cell lines. (Faculty of Sciences of University of Lisbon, 2023).
72. Bergdorf, K. N. *et al.* Immunofluorescent staining of cancer spheroids and fine-needle aspiration-derived organoids. *STAR Protocols* **2**, 100578 (2021).
73. Melo, C. E. M. de. The impact of Lama2-deficiency on cell cycle regulation and survival. (2022).
74. Papes, F. *et al.* Transcription Factor 4 loss-of-function is associated with deficits in progenitor proliferation and cortical neuron content. *Nat Commun* **13**, 2387 (2022).
75. Preibisch, S., Saalfeld, S. & Tomancak, P. Globally optimal stitching of tiled 3D microscopic image acquisitions. *Bioinformatics* **25**, 1463–1465 (2009).
76. Cerami, E. *et al.* The cBio cancer genomics portal: an open platform for exploring multidimensional cancer genomics data. *Cancer Discov* **2**, 401–404 (2012).
77. de Bruijn, I. *et al.* Analysis and Visualization of Longitudinal Genomic and Clinical Data from the AACR Project GENIE Biopharma Collaborative in cBioPortal. *Cancer Res* **83**, 3861–3867 (2023).
78. Gao, J. *et al.* Integrative analysis of complex cancer genomics and clinical profiles using the cBioPortal. *Sci Signal* **6**, pl1 (2013).
79. Weinstein, J. N. *et al.* The Cancer Genome Atlas Pan-Cancer Analysis Project. *Nat Genet* **45**, 1113–1120 (2013).
80. Petrov, P. B., Considine, J. M., Izzi, V. & Naba, A. Matrisome AnalyzeR – a suite of tools to annotate and quantify ECM molecules in big datasets across organisms. *Journal of Cell Science* **136**, jcs261255 (2023).
81. WANG, G.-H. *et al.* Identification of MXRA5 as a novel biomarker in colorectal cancer. *Oncol Lett* **5**, 544–548 (2013).
82. Xiong, D. *et al.* Exome sequencing identifies MXRA5 as a novel cancer gene frequently mutated in non–small cell lung carcinoma from Chinese patients. *Carcinogenesis* **33**, 1797–1805 (2012).
83. Sun, J.-Z. *et al.* MXRA5 Is a Novel Immune-Related Biomarker That Predicts Poor Prognosis in Glioma. *Dis Markers* **2021**, 6680883 (2021).
84. Gilbert, L. A. *et al.* Genome-Scale CRISPR-Mediated Control of Gene Repression and Activation. *Cell* **159**, 647–661 (2014).
85. Heidersbach, A. J., Dorighi, K. M., Gomez, J. A., Jacobi, A. M. & Haley, B. A versatile, high-efficiency platform for CRISPR-based gene activation. *Nat Commun* **14**, 902 (2023).
86. Javaid, N., Pham, T. L. H. & Choi, S. Functional Comparison between VP64-dCas9-VP64 and dCas9-VP192 CRISPR Activators in Human Embryonic Kidney Cells. *International Journal of Molecular Sciences* **22**, 397 (2021).
87. Ohguro, H. *et al.* STAT3 Is the Master Regulator for the Forming of 3D Spheroids of 3T3-L1 Preadipocytes. *Cells* **11**, 300 (2022).
88. Xiao, H. *et al.* Identification and functional activity of matrix-remodeling associated 5 (MXRA5) in benign hyperplastic prostate. *Aging (Albany NY)* **12**, 8605–8621 (2020).
89. Decarli, M. C. *et al.* Cell spheroids as a versatile research platform: formation mechanisms, high throughput production, characterization and applications. *Biofabrication* **13**, 032002 (2021).
90. Conceição, A. Understanding the Impact of alterations in the expression of LAMA2 in melanoma. (NOVA University Lisbon, 2023).
91. Martins, S. G. *et al.* Laminin-α2 chain deficiency in skeletal muscle causes dysregulation of multiple cellular mechanisms. *Life Science Alliance* (Accepted for publishing) (2024) doi:10.1101/2024.01.20.576409.

92. Gutbier, S. *et al.* Major changes of cell function and toxicant sensitivity in cultured cells undergoing mild, quasi-natural genetic drift. *Arch Toxicol* **92**, 3487–3503 (2018).
93. Li, J., Settivari, R. S. & LeBaron, M. J. Genetic instability of in vitro cell lines: Implications for genetic toxicity testing. *Environmental and Molecular Mutagenesis* **60**, 559–562 (2019).
94. Torsvik, A. *et al.* U-251 revisited: genetic drift and phenotypic consequences of long-term cultures of glioblastoma cells. *Cancer Medicine* **3**, 812–824 (2014).
95. Zhang, A., Miao, K., Sun, H. & Deng, C.-X. Tumor heterogeneity reshapes the tumor microenvironment to influence drug resistance. *Int J Biol Sci* **18**, 3019–3033 (2022).
96. Brady, L. *et al.* Inter- and intra-tumor heterogeneity of metastatic prostate cancer determined by digital spatial gene expression profiling. *Nat Commun* **12**, 1426 (2021).
97. Wu, F. *et al.* Single-cell profiling of tumor heterogeneity and the microenvironment in advanced non-small cell lung cancer. *Nat Commun* **12**, 2540 (2021).
98. Erdogan, B. *et al.* Cancer-associated fibroblasts promote directional cancer cell migration by aligning fibronectin. *J Cell Biol* **216**, 3799–3816 (2017).
99. Han, S. W. & Roman, J. Fibronectin induces cell proliferation and inhibits apoptosis in human bronchial epithelial cells: pro-oncogenic effects mediated by PI3-kinase and NF-kappa B. *Oncogene* **25**, 4341–4349 (2006).
100. Lin, T.-C. *et al.* Fibronectin in Cancer: Friend or Foe. *Cells* **9**, 27 (2020).
101. Yao, Y. Laminin: loss-of-function studies. *Cell. Mol. Life Sci.* **74**, 1095–1115 (2017).
102. Thyboll, J. *et al.* Deletion of the Laminin α4 Chain Leads to Impaired Microvessel Maturation. *Molecular and Cellular Biology* **22**, 1194–1202 (2002).
103. Barraza-Flores, P. *et al.* Laminin-111 protein therapy enhances muscle regeneration and repair in the GRMD dog model of Duchenne muscular dystrophy. *Hum Mol Genet* **28**, 2686–2695 (2019).
104. Rooney, J. E., Knapp, J. R., Hodges, B. L., Wuebbles, R. D. & Burkin, D. J. Laminin-111 protein therapy reduces muscle pathology and improves viability of a mouse model of merosin-deficient congenital muscular dystrophy. *Am J Pathol* **180**, 1593–1602 (2012).
105. Kortylewski, M., Jove, R. & Yu, H. Targeting STAT3 affects melanoma on multiple fronts. *Cancer Metastasis Rev* **24**, 315–327 (2005).
106. Ribeiro, V. F. L. How Lama2-deficiency impacts myoblast differentiation in a mouse model for LAMA2-congenital muscular dystrophy. (Faculty of Sciences of University of Lisbon, 2022).
107. Lin, T., Lin, Z., Mai, P., Zhang, E. & Peng, L. Identification of prognostic biomarkers associated with the occurrence of portal vein tumor thrombus in hepatocellular carcinoma. *Aging (Albany NY)* **13**, 11786–11807 (2021).
108. Horejs, C.-M. Basement membrane fragments in the context of the epithelial-to-mesenchymal transition. *European Journal of Cell Biology* **95**, 427–440 (2016).
109. Singh, M., Yelle, N., Venugopal, C. & Singh, S. K. EMT: Mechanisms and therapeutic implications. *Pharmacology & Therapeutics* **182**, 80–94 (2018).
110. Peng, S. *et al.* Identification of matrix-remodeling associated 5 as a possible molecular oncotarget of pancreatic cancer. *Cell Death Dis* **14**, 1–14 (2023).

6. Annex

Table S1– List of gRNA oligonucleotides.

gRNA Oligonucleotides	Sequence (5' - 3')
CRISPRa1 Forward	CACCGTTTAATAGAGGGCCGTCCTG
CRISPRa1 Reverse	AAACCAGGACGGCCCTCTATTAAAC
CRISPRa2 Forward	CACCGAGGTCAAGCTAGGAATGATC
CRISPRa2 Reverse	AAACGATCATTCCTAGCTTGACCTC
CRISPRa3 Forward	CACCGAAAGGAGGATCCTTTAATAG
CRISPRa3 Reverse	AAACCTATTAAAGGATCCTCCTTTC
Scramble Forward [74]	CACCGAAATGTGAGATCAGAGTAAT
Scramble Reverse [74]	AAACATTACTCTGATCTCACATTTC

Table S2 – List of antibodies used in spheroid immunofluorescence.

Antibody	Application	Raised in	Primary vs Secondary	Dilution	Catalogue number	Brand
Laminin alpha2 chain	Immunofluorescence	Rat	Primary	1:100	L0663	Sigma
Fibronectin	Immunofluorescence	Rabbit	Primary	1:200	F-3648	Sigma
Pan-laminins	Immunofluorescence	Rabbit	Primary	1:100	L- 9393	Sigma
Anti-rabbit IgG Alexa 488	Immunofluorescence	Goat	Secondary	1:500	A-11070	Invitrogen
Anti-rat IgG Alexa 568	Immunofluorescence	Goat	Secondary	1:500	A-11077	Invitrogen
STAT3	Western Blot	Rabbit	Primary	1:1000	126405	Cell Signalling Technology
p-STAT3 Y705	Western Blot	Rabbit	Primary	1:1000	91455	Cell Signalling Technology
GADPH	Western Blot	Rabbit	Primary	1:1000/1:2000	2118S	Cell Signalling Technology
Anti-rabbit IgG-HRP	Western Blot	Donkey	Secondary	1:5000	NA934	GE Healthcare

Table S3 – List of solutions used in spheroid immunofluorescence.

Solution	Composition
1x TBST (concentrated Tris- Buffered Saline with Tween-20)	48g Tris base, 176 g NaCl, dissolve in 5L of dH_2O, pH 7.4-7.6 with HCI, dH_2O to a final volume of 20L, 20 ml of Tween-20
0.1% TBSTX	0.1% Triton-X100 in 1XTBST
0.5% TBSTX	0.5% Triton X-100 in 1X TBST
Blocking Solution	2% BSA in 0.1% TBSTX
Mowiol-DABCO	2.4g of Mowiol, 4.8 mL of 100% glycerol and 2.5% DABCO in H_2O, pH 8.5 with 0.2M Tris-HCl

Table S4 – List of primers used for qPCR.

Gene	Primer	Sequence (5' - 3')	Amplicon Size
LAMA2	Forward	TGAGTATGAAAGCAAGGCCAGA	186
	Reverse	GGGAGAGCTCCACAAAACCA	
ACTIN B	Forward	GAGCACAGAGCCTCGCCTT	70
	Reverse	TCATCATCCATGGTGAGCTGG	
MXRA5	Forward	CGACGCGCTCTTCAGTTTTG	179
	Reverse	TGTGTTCAATCTTGGCCGGT	
MAPK6	Forward	TGACTGAGCCACACAAACCT	73
	Reverse	TGTTCCAGGAAATCCAGTGCTTC	

Table S5 – qPCR protocol.

qPCR System	BioRad CFX96TM	
Setting/Mode	SYBR only	
Polymerase Activation and DNA Denaturation	30 seconds at 95ºC	
Amplification	Denaturation at 95ºC	5 seconds
	Annealing/Extension and Plate Read at 60ºC	15 seconds
	Cycles	40
Melting Curve Analysis	65-95ºC	
	0.5ºC increments at 5 seconds/step	

Table S6– Primers used for Sanger sequencing of *LAMA2* promotor region.

Sanger Sequencing	Sequence (5' - 3')
LAMA2_OE_ gRNA_validation_Fwd	CAGGCCTTTCTCAAGAGGTAAA
LAMA2_OE_ gRNA_validation_Rev	GAGAAAGAGGACACTCCTCCAC

Table S7 – Q5 High Fidelity PCR protocol.

Step	Temperature (ºC)	Time	
1	98	30 sec	
2	98	5-10 sec	
3	63	10-30 sec	
4	72	8 sec	20-30 sec/kb
5			Repeat steps 2-4 for 30 cycles
6	72	2 min	
7	4		Hold

Table S8– Forward primer used for colony PCR.

Colony PCR	Sequence (5' - 3')
pX330_U6_seq_fwd [73]	AGTACAAAATACGTGACGTAG

Table S9 – Colony PCR protocol

Step Number	Temperature (ºC)	Time	
1	94	2 min	
2	94	20 sec	
3	65	15 sec	-0.5 ºC per cycle decrease
4	68	10 sec	
5			Repeat steps 2-4 for 10 cycles
(Touchdown)			
6	94	15 sec	
7	60	15 sec	
8	72	10 sec	
9			Repeat steps 6-8 for 28 cycles
10	72	2 min	
11	12		Hold

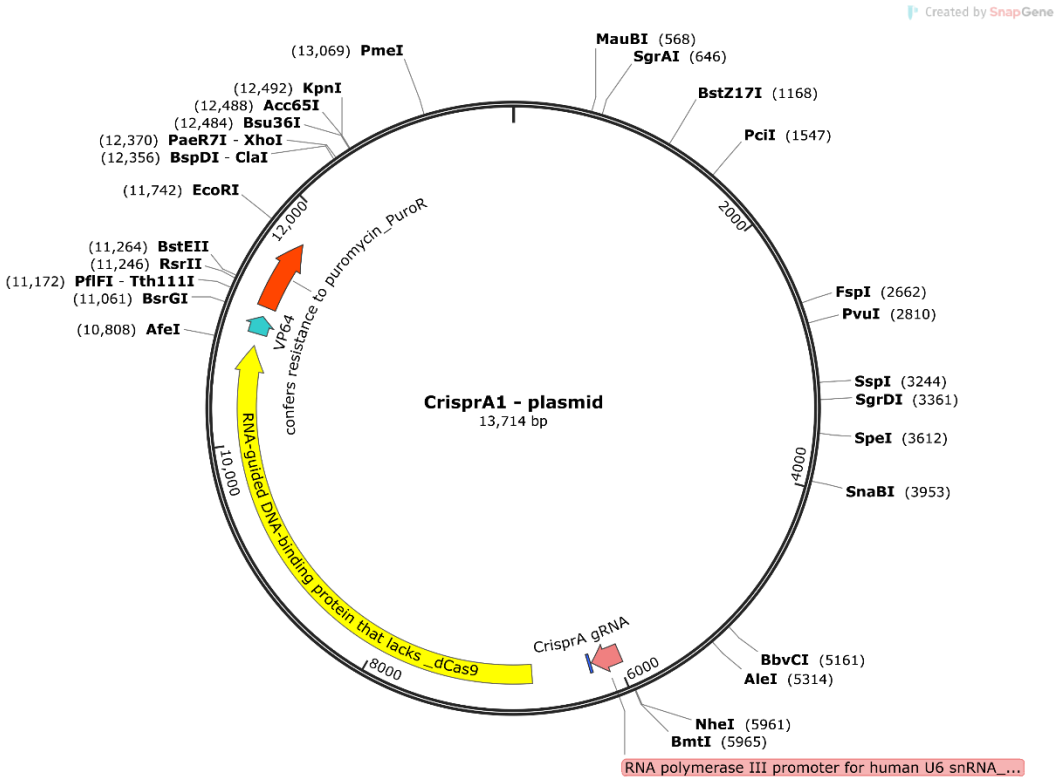

Figure S1 – LentisamV2 backbone used to generate OEA1, OEA2, OEA3 and scramble plasmids.

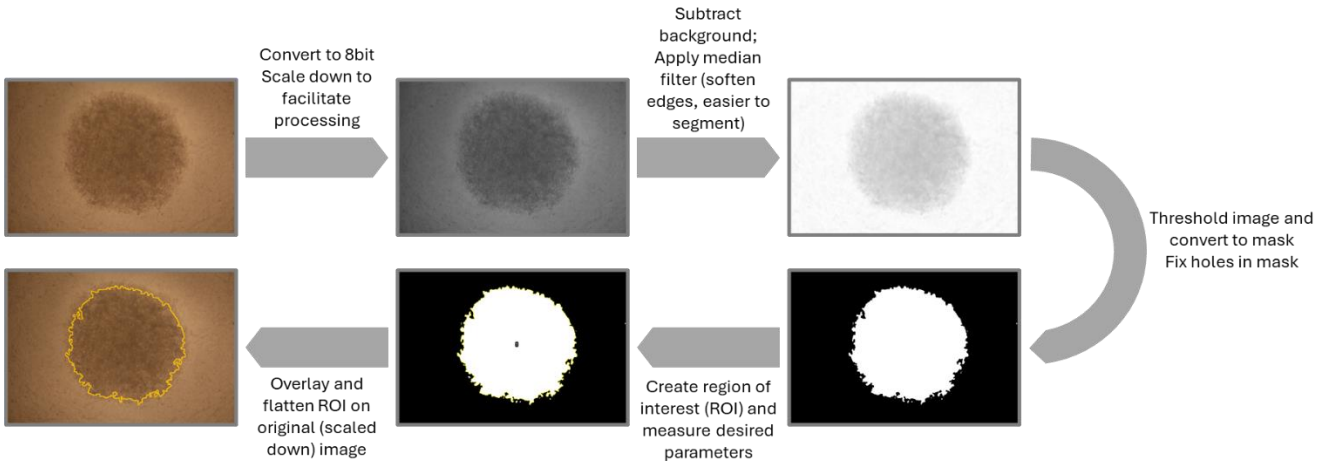

Figure S2 – Schematic representation of the custom ImageJ script for spheroid segmentation and area measurement.

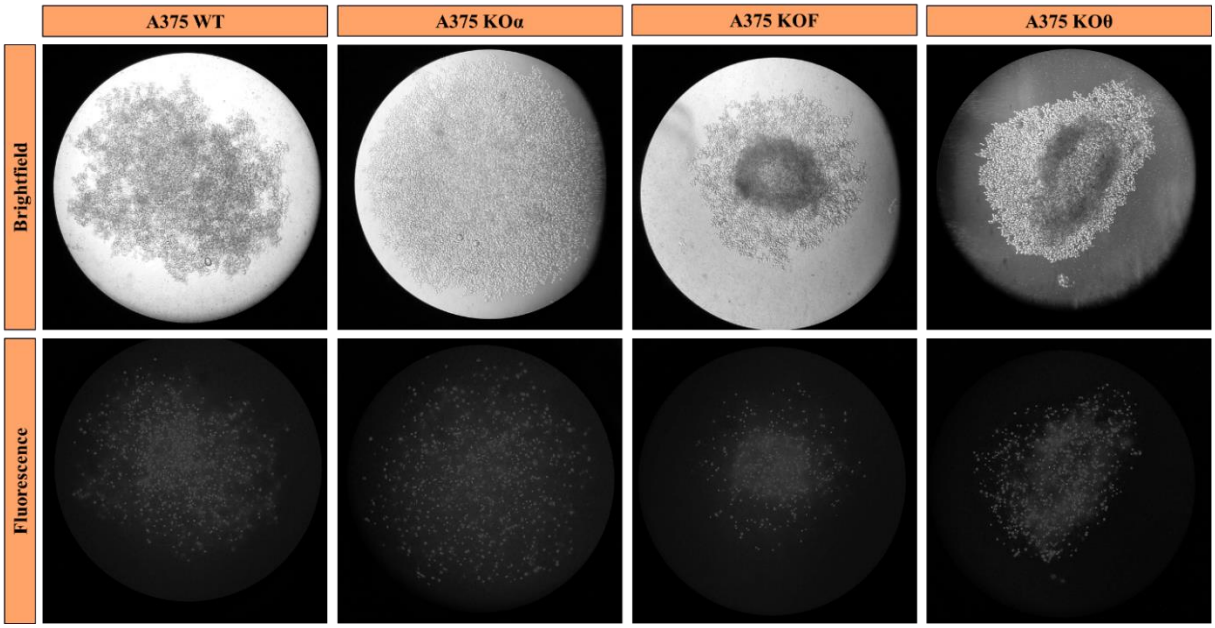

Figure S3 – PI-stained spheroids.